Evaluation of Ride Comfort and Road Holding for Heavy Vehicle Suspension (HVS) through Model Predictive Controller (MPC) based on Hybrid Semi-Active Damping Strategy

by

Michael Faronbi O.

A Project Submitted in Partial Fulfillment of the
Requirement for the Degree of

MASTER OF ENGINEERING

In the Department of Engineering

University of Victoria

We acknowledge and respect the lək^{w}əŋən peoples on whose traditional territory the university stands and the Songhees, Esquimalt and W̱SÁNEĆ peoples whose historical relationships with the land continue to this day.

Abstract

The continuous expansion of industrial demand in various countries has increased the need for large commercial vehicles to transport products between locations. As a result, freight transportation has become a key driver of economic growth, contributing significantly to a country's GDP, typically accounting for 6-12% of the total. However, this rapid growth in road transportation has also brought about a rise in traffic congestion and a higher probability of road accidents. According to a European Union assessment, large vehicles are a significant factor in these incidents. Nevertheless, the primary cause of road accidents remains driver negligence.

Work-related injuries and disorders caused by whole-body vibration have been extensively studied worldwide. To address this problem, researchers have developed a pitch plane model of a large vehicle using a Lagrangian approach coupled with various hybrid semi-active damping schemes based on the model predictive control (MPC) framework. The MPC-based suspension controller is designed to optimize comfort and handling by minimizing a quadratic cost function.

The focus has been on reducing the vertical accelerations experienced by the vehicle due to variations in the vehicle and road profile to improve the vehicle's stability and ride comfort level. Additionally, managing the changes in vertical force encountered by each tire during its interaction with the road has been crucial. The ride comfort of the driver has been evaluated by analyzing the vertical accelerations at the center of gravity of the pitch plane model, both with and without the MPC-based controller, using the guidelines specified in ISO 2631-1/2.

Simulation results have demonstrated the impact of the MPC-based controller, with and without its implementation, on the ride comfort level and road-holding capability of the heavy

vehicle system. These findings highlight the potential of the MPC-based controller to enhance the overall performance of heavy vehicle systems in terms of ride comfort and road holding.

Keywords: *heavy vehicle, ride comfort, road holding, MPC-based controller, suspension, industrial demand, freight transportation, road accidents, whole-body vibration, Lagrangian approach, model predictive control.*

TABLE OF CONTENTS

LIST OF FIGURES

LIST OF TABLES

LIST OF ABBREVIATIONS

AAP	Average Absorbed Power
DOF	Degrees of Freedom
DOE	Design of Experiment
DQ	Differential Quadrature
FEM	Finite Element Method
FFT	Fast Fourier Transformation
FRFs	Frequency Response Function
HY-GH-SH	Hybrid Grounddhook Skyhook
HY-B-SH	Hybrid Balance Skyhook
HY -B-GH	Hybrid Balance Groundhook
HY-GH-SH-B	Hybrid Groundhook Skyhook Balance
ISO	International Standard Organization
LTI	Linear Time-Invariant
PLC	Programmable Logic Controller
RMS	Root Mean Square
RPM	Rotation Per Minute
RC	Ride Comfort
HBM	Human Body Model
FFT	Fast Fourier Transform

NOMENCLATURES

a_n	maximum accelration value
A_{irms}	RMS acceleration value
A	area of cross-section
A_n	slowly varying function of time
a_{wi}	frequency weighted acceleration
C_s^f	damping coefficient of front damper
C_s^r	damping coefficient of rear damper
$C_{skyhook}$	skyhook damping coefficient
C_{on}	on-state damping
$C_{\max}, C_{\min}$	maximum and minimum damping coefficient
C_{gnd}	damping coefficient of groundhook damper
EI	flexural rigidity
$F_{balance}$	damping force of the balance logic damper
$F_{skyhook}$	skyhook damping force of the skyhook damper
$F_{groundhook}$	damping force of the groundhook damper
G_d	PSD of vertical displacement
G	system
$h(x)$	simple harmonic function of road profile
h	height of bump
I_d	roatrary inertia
I	current
J	pitch inertia
K_I	coefficient for integral term
K_s	suspension stiffness
K_t	tire stiffness

K_{i}	weighted coefficient
L	Beam length
L_b	length of bump
M	center of mass
M_s	sprung mass
M_{us}	unsprung mass
n	spatial frequency
Δn	frequency band
$N_{\exp}$	total number of experiments
u	control force
U	Amplitude of vibration
V	velocity input
$W(x)$	eigen-function
w	transverse displacement
W_k	weighted acceleration
W_d	weighted acceleration for horizontal acceleration (Lognitudinal and lateral)
W_b	weighing factor for vertical acceleration
$x_1, \dot{x}_1, \ddot{x}_1$	vertical displacement,velocity, acceleration of sprung mass
$x_2, \dot{x}_2, \ddot{x}_2$	vertical displacement , velocity, acceleration of unsprung mass

Greek Symbols

ρ	mass denisity
α	significance level
β	second order regression coefficient
ω	eigenfrequency
η	umbra time
ω_n	natural frequency
a_i	RMS acceleration
Ω	Angular spatial frequency

Ω_0	Initial angular spatial frequency
θ	Pitch velocity

Chapter 1
Introduction

1.1 Background and Motivation

Evaluating ride comfort and road holding for heavy vehicle suspension (HVS) is paramount in automotive engineering. Heavy vehicles play a critical role in various industries with the increasing demand for efficient and reliable transportation of goods. However, these vehicles often face challenges in providing a smooth and comfortable ride, especially when navigating uneven road surfaces or encountering external disturbances. The suspension system of heavy vehicles is responsible for mitigating the impact of road irregularities, ensuring the safety and comfort of the occupants, and protecting the transported goods. While simple and cost-effective, traditional passive suspension systems often fall short in delivering optimal ride comfort and road handling characteristics. There is growing interest in developing semi-active suspension systems that dynamically adjust real-time damping attributes based on road conditions and vehicle dynamics. Model predictive control (MPC) is a potential method for managing semi-active suspension systems that enables proactive damping force modification for enhanced ride comfort and road holding.

The hybrid semi-active damping strategy, combining passive and active damping elements, presents an intriguing approach to enhance the performance of heavy vehicle suspensions. By utilizing a combination of passive components for load carrying and active elements for damping adjustment, this strategy aims to strike a balance between comfort and handling characteristics. Therefore, the motivation for this thesis is to thoroughly investigate the evaluation of ride comfort and road holding for heavy vehicle suspension through a model predictive controller based on a hybrid semi-active damping strategy. This research aims to

contribute to the existing knowledge by providing insights into the design, implementation, and control of such suspension systems, ultimately leading to improved ride comfort, road holding, and vehicle performance for heavy vehicles.

Traditionally, trucks have a primary suspension between the axles and chassis and a secondary suspension system for the cabin and driver seat [1]. The secondary suspension system provides ride comfort without compromising the handling and stability of the vehicle. Over time, the cabin suspension has improved with various materials such as fixed cab mounts, rubber bushings, steel springs, and air springs. The air spring suspension offers larger suspension travel, lower isolation frequencies, and the ability to adjust for changes in cabin load.

An upgrade from passive suspension systems with the use of semi-active or active suspension systems. Passive suspension elements such as springs and dampers can only store or dissipate energy. In contrast, semi-active suspension systems can add energy and adjust their characteristics using a small amount of external energy [2]. On the other hand, active suspension systems use actuators to provide the desired ride characteristics by applying controlled forces to the suspended mass through a system controller [3]. However, the energy consumption of active suspension systems is typically high. Semi-active suspension systems offer a balance between performance potential and energy consumption.

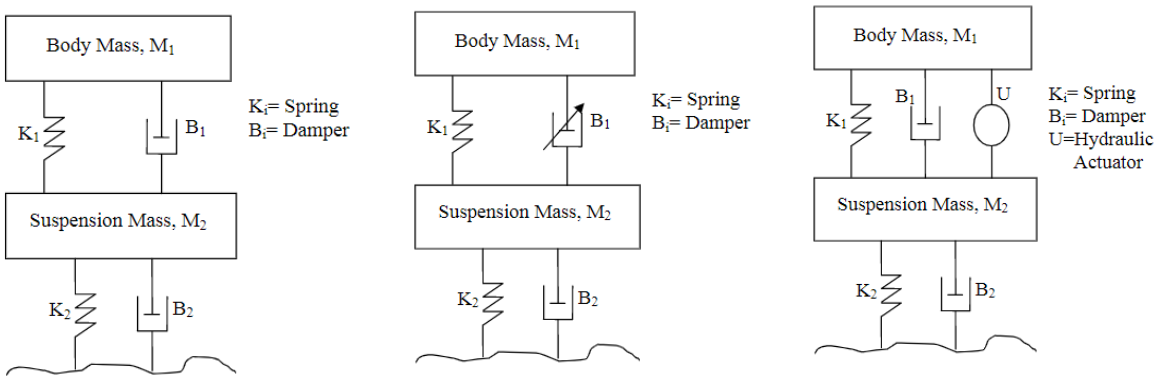

Passive System | Semi-Active System | Active system

Table 1.1: Showing passive system, semi-active system, and active system.

Semi-active suspension systems are a good compromise between active and passive suspension systems as they can store and dissipate energy at a rate that allows for quick changes in suspension characteristics, thus resulting in improved ride comfort [4]. However, the disadvantage is that they still require a certain amount of energy consumption compared to passive suspension systems [5,6].

The thesis proposes a model-based control strategy that considers the realistic framework of the semi-active suspension system and aims to utilize its potential fully. The control strategy ensures compatibility and transparency in modeling and controller design, making the system easier to understand and manage. The proposed controllers have low complexity and intuitive structures, making them comparable to established controllers.

The thesis also presents two control approaches based on optimality; however, these approaches are not yet suitable for industrial applications due to their high computation time [7]. Despite this, the thesis provides a comprehensive review of literature, including recent developments in heavy vehicle dynamics, to thoroughly understand the current state-of-the-art in this field [8,9].

1.2 Literature Review

In recent years, the study of heavy vehicle dynamics has become a prominent focus in mechanical engineering. This research encompasses a range of topics, including the dynamic modeling of trucks, the development of suspension control systems, and the enhancement of ride comfort and road holding capabilities. Crucial to these studies is creating a comprehensive mathematical model that represents the truck's structure. Such a model typically includes elements like the cabin, suspension system, tires, and the influence of road surface irregularities. These models are pivotal in analyzing truck dynamics, particularly in understanding how chassis vibrations, primarily dictated by road conditions, can be mitigated through advanced suspension designs.

Margolis [10,11] has been instrumental in exploring heavy vehicles' structural aspects and dynamic characteristics. In 1996, Ibrahim et al. [12] delved into the study of truck vibrations during transit, paying particular attention to how the flexural rigidity of the vehicle impacts the comfort experienced by the driver. They utilized finite element method (FEM) techniques to model the vehicle and assess its modal properties. Similarly, Kiencke and Daib (1997) [13] researched vehicles' linear and nonlinear dynamics, mainly focusing on tire side-slip angles. They created a linear observer to facilitate comparisons in their study.

Extending these investigations, Carlbom, in 2000 and 2001 [14,15,16], assessed the effect of structural flexibility on the ride quality of road vehicles and their overall dynamics. His approach involved both measurements and simulations, leading to the proposal of four distinct criteria designed to streamline FEM modeling and enhance the efficiency of simulations.

Margolis contributed significantly in 2001 [17] by developing a bondgraph model that integrates sensors, actuators, and vehicle dynamics to devise vehicle safety controls. This model simulated human body motion in six directions, including a representation of the front

steering mechanism, and mimicked the effects of the suspension on the vehicle, alongside incorporating data on road characteristics.

In the same year, Margolis and Shim [16] innovated a nonlinear vehicle dynamic model for a four-wheel vehicle equipped with electrically controlled brakes, steering, and individual suspension controllers. Additionally, in 2005, Li and Sandu [18] introduced an algorithm for assessing the tractive capacity of off-road vehicles by considering rapidly changing external excitations and their effects on the vehicle.

In 2005 [19], Cao advocated for a trio of modeling approaches in truck dynamics. These included discrete modeling of the chassis with preliminary assumptions and calculations, the estimation or measurement of modal masses and stiffness, and the comprehensive FEM modeling of the entire vehicle.

Kiencke et al. 2007 [20] explored lateral vehicle dynamics, continuing this innovation trend. Their study focused on detecting critical driving situations and estimating adhesion characteristics during cornering, comparing the effectiveness of linear and nonlinear observers in these scenarios.

Fischer et al. (2007) [21] ventured into stabilising horizontal and vertical motions in vehicles to prevent unstable or unpredictable behaviours. Their work highlighted the need for improved fault detection and diagnosis methods due to the complexities introduced by adding various actuators and sensors in modern vehicles.

In the study by Teng et al. (2008) [22], a multi-body dynamics method was applied to study vehicle frontal collisions, creating a 15-part model representing a hybrid dummy. This research proved crucial for assessing vehicle crash safety and advancing safety technologies. Zhou et

al. (2009) [23] formulated an analytical model of a car body to explore how frame damping influences vertical stiffness and affects the vehicle's vibrational behavior.

Furthermore, Huong et al. (2010) developed a model focusing on the vertical vibrations experienced in high-speed railway passenger cars. Their model treated the car as an Euler beam with free ends, revealing that the primary bending mode of the car body notably impacts passenger comfort. Tomioka et al. (2017) [25] delved into how suspension damping influences railway passenger car dynamics. Their study, which included various tests under different conditions, evaluated the effect of damping on the vertical oscillations of these vehicles and employed a specific method to calculate the average RMS value.

$$S_{rms} = \frac{1}{N}\sum_{n=1}^{N} P_{rms} \tag{1.1}$$

Dumitui et al. (2017) [26] developed a computational model of a railway car using the finite element method (FEM) and a flexible body model. By comparing the responses of the flexible body model with the rigid body response, the study demonstrated the effectiveness and validity of the computation model.

The previous section has outlined the substantial research on modeling rail and road vehicles. In the following section, we will explore the existing literature about advancements in suspension control.

Control Evaluation

Several studies have compared the performance of semi-active suspension systems with conventional passive systems. Karnoop et al. (1974) [27] compared skyhook-controlled semi-active and traditional passive systems. Karnopp (1990) [28, 29] further contributed to the research in this area. Semi-active systems offer the advantages of active systems with lower energy consumption and increased reliability compared to passive systems.

In the late 1980s, Alanoly and Sankar [30, 31] researched the application of balance logic for vibration and shock isolation. Liu et al. (2005) [32] compared the "on-off" and "continuous" skyhook and balance logics with an adaptive passive damping control system. Shamsi and Choupani (2008) [33] presented on-off and continuous skyhook control for a half-car roll plane model and compared its frequency and transient responses to a passive system. Strecker et al. (2015) [34] conducted a study comparing three semi-active control algorithms (groundhook, skyhook, and modified groundhook) with a passive system.

The efficiency of the semi-active suspension system was evaluated through simulations using different response times of a magneto-rheological (MR) damper. Response times of 1.5 ms, 8 ms, and 20 ms were tested to understand the impact of the damper's response time on the overall performance of the suspension. The algorithms employed in the study are also presented.

$$\text{Groundhook: } F_{gh} = \begin{cases} c_{max}(\dot{x}_1 - \dot{x}_2), & (\dot{x}_2 - \dot{x}_{in})(\dot{x}_1 - \dot{x}_2) < 0 \\ c_{min}(\dot{x}_1 - \dot{x}_2), & (\dot{x}_2 - \dot{x}_{in})(\dot{x}_1 - \dot{x}_2) \geq 0 \end{cases} \tag{1.2}$$

$$\text{Skyhook: } F_{sa} = \begin{cases} c_{max}(\dot{x}_1 - \dot{x}_2), & \dot{x}_1(\dot{x}_1 - \dot{x}_2) \geq 0 \\ c_{min}(\dot{x}_1 - \dot{x}_2), & \dot{x}_1(\dot{x}_1 - \dot{x}_2) < 0 \end{cases} \tag{1.3}$$

Modified Groundhook:

$$F_{ghmod} = \begin{cases} c_{max}(\dot{x}_1 - \dot{x}_2), & \ddot{x}_2(\dot{x}_1 - \dot{x}_2) \geq 0 \\ c_{min}(\dot{x}_1 - \dot{x}_2), & \ddot{x}_2(\dot{x}_1 - \dot{x}_2) < 0 \end{cases} \tag{1.4}$$

The study showed that the modified groundhook approach enhanced the magneto-rheological (MR) damper effectiveness, particularly with shorter response times (1.5ms), and also marginally increased comfort compared to passive systems even with longer response times (20ms). The skyhook control strategy's impact on suspension quality was less dependent on response time, maintaining comfort levels even at 20ms. Generally, shorter response times correlated with improved overall performance.

In their 2015 research, Bakar et al. broadened the scope of control algorithms by evaluating skyhook and modified skyhook strategies within a fully modeled car. This analysis aimed to mitigate the water hammer effect observed in the modified skyhook approach. The modified skyhook control combined elements from passive and standard skyhook damping systems by adopting a hybrid approach.

$$If\ v_1 v_{12} \geq 0\ then\ F_d = c_{sky} v_1 \qquad (1.5)$$
$$If\ v_1 v_{12} < 0\ then\ F_d = 0$$

In the study, v_1 represents the velocity of the sprung mass, v_{12} represents the difference in velocity between the sprung and unsprung masses, F_d denotes the damping force, and c_{sky} represents the skyhook damping constant. The logic may be given as,

$$F_d = c_{ms}\left[\alpha\left(\dot{Z}_u - \dot{Z}_s\right) + (1-\beta)\dot{Z}_s\right] \qquad (1.6)$$

In the revised interpretation of the skyhook logic, the damping constant is denoted by c_{ms} while β represents the passive-to-skyhook damping ratio. Additionally $\dot{Z}_u$, $\dot{Z}_s$ symbolize the velocities of the unsprung and sprung masses, respectively. The efficacy of semi-active suspension systems is intricately linked to the control algorithm employed. Studies have shown that under random road conditions, the skyhook control algorithm performance exceeds that of the modified skyhook algorithm by a margin of 3.2%. However, in scenarios involving vertical and roll movements, the modified skyhook algorithm demonstrates superior effectiveness compared to the traditional skyhook approach.

In their 2013 research, Hailong and et al. [35] explored the semi-active control of full vehicle suspension systems using the skyhook principle, incorporating magneto-rheological (MR) dampers. The team developed a comprehensive 7-degree-of-freedom (DOF) dynamic model for the entire vehicle, integrating the modified Bouc-Wen hysteretic model specifically for the

MR dampers. This study utilized the modified skyhook control strategy enabling independent management of the four MR quarter vehicle subsystems.

$$i_{di} = \begin{cases} k_d|\dot{x}_{si}|^m, & \dot{x}_{si}(\dot{x}_{si} - \dot{x}_{ui}) > 0, \\ 0, & \dot{x}_{si}(\dot{x}_{si} - \dot{x}_{ui}) \leq 0, \end{cases} \quad i = 1, 2, 3, 4, \tag{1.7}$$

Hailong et al 2013 research [35] focused on comparing the efficacy of a Magneto-Rheological (MR) semi-active suspension system with its passive counterpart. Utilizing a sophisticated 7-DOF dynamic model for the entire vehicle and an adapted Bouc-Wen hysteretic model tailored for the MR damper the investigation delved into the vertical movement attributes of the suspension system. Through the application of harmonic excitations coupled with delay times, it was observed that the MR system peak acceleration reduced notably by 30% in comparison to the passive system. However, it is important to note that the MR system unsprung mass reacted more abruptly hinting at a possible trade-off in terms of road handling and comfort. Despite this, a decrease in both pitch and roll angular acceleration was noted in the MR system suggesting an enhancement in the overall ride quality. The study also explored the MR system shock isolation proficiency employing rounded pulse excitations. The findings highlighted the MR system superior shock isolation capabilities relative to the passive system. Additionally, the MR system showed promising potential in dampening low-frequency resonances (ranging from 0.5 to 2.0 Hz) under random road conditions, an indication of its capability to markedly elevate suspension performance particularly in diminishing lower frequency vibrations.

In a subsequent investigation by Amin et al. in 2015 [36], a skyhook logic controller was scrutinized for its application in a 7-DOF ride model of an armored vehicle. This controller consisted of dual loops; the first aimed at managing the vehicles body, pitch, and roll accelerations due to road disturbances while the second was responsible for modulating

damping characteristics. The system employed a PID control mechanism in the outer loop coupled with skyhook logic in the inner loop to regulate the damping force effectively.

$$F_{sa} = -c_{sa}(\dot{x}_2 - \dot{x}_1) = -c_{sky}\dot{x}_1 \quad (1.8)$$

Where, F_{sa} is the damping force, c_{sa} is the semi- active damping coefficient, c_{sky} is the skyhook damping coefficient, $\dot{x}_1$ is the sprung mass velocity and $\dot{x}_2$ is the unsprung mass velocity. Raj et al. (2015) [37] conducted a study focusing on the application of a fuzzy logic controller based on skyhook logic to regulate a semi-active suspension system for a high mobility multipurpose wheeled vehicle (HMMWV). The fuzzy logic controller, based on multi-valued logic and the capability to operate between high and low damping states, utilized the sprung mass velocity and relative velocity as system inputs and controlled the damping coefficient of the controllable damper as the output. The evaluation of the system performance involved subjecting it to a sinusoidal road input.

The study highlighted notable enhancements in vehicle dynamics when applying a fuzzy logic controller based on continuous skyhook logic, along with fuzzy PID and semi-active suspension. This approach outperformed traditional on-off skyhook and passive systems. Specifically, the fuzzy controller utilizing continuous skyhook logic excelled in reducing sprung mass displacement and acceleration, while the integration of PID control in the fuzzy logic system significantly ameliorated ride comfort by effectively moderating velocity fluctuations.

Hybrid Control Strategies

Strydom et al. (2014) [38] investigated the application of hybrid control in a compact off-road vehicle. This vehicle was equipped with a suspension system that combined adjustable dampers with conventional spring-damper units. They developed a comprehensive 12-DOF dynamic

model and applied both skyhook and groundhook control mechanisms. The skyhook control notably enhanced ride comfort but had the drawback of increasing unsprung mass motion. In contrast, groundhook control was more effective in road handling but at the expense of ride comfort. To address this, the study employed adaptive control techniques to optimize the relative velocity across the damper.

$$\begin{aligned} \dot{Z}_s\dot{x}_{cl} > 0: &\quad \sigma_{sky} = \dot{Z}_s \\ \dot{Z}_s\dot{x}_{cl} \leq 0: &\quad \sigma_{sky} = 0 \\ \dot{Z}_u\dot{x}_{cl} < 0: &\quad \sigma_{gnd} = -\dot{Z}_u \\ \dot{Z}_u\dot{x}_{cl} \geq 0: &\quad \sigma_{gnd} = 0 \end{aligned} \tag{1.8}$$

In the study, $\dot{Z}_s$ represents the velocity of the sprung mass, $\dot{Z}_u$ represents the velocity of the unsprung mass, σ_{sky} and σ_{gnd} (control inputs) for the semi-active force $F_{SA,z}$, is determined by the skyhook and groundhook control inputs.

$$F_{SA,z} = G\left[a\sigma_{sky} + (1-a)\sigma_{gnd}\right] \tag{1.9}$$

In their 2015 research, Kashem and colleagues [39] introduced a novel approach to semi-active vehicle suspension systems focusing on a continuous skyhook mechanism with adaptable gain settings. They rigorously evaluated eleven different suspension configurations, emphasizing the enhancement of peak amplitude and settling times. This process involved initially halting road input and then determining the most effective skyhook gain, followed by the application of a newly developed skyhook control algorithm. Notably, employing a skyhook logic with a gain parameter set at 1200 Ns/m markedly enhanced ride comfort. Conversely, the implementation of groundhook logic was found to effectively diminish the wheels' vertical acceleration, contributing to better road holding. Among the tested configurations, a system with low damping and without control exhibited the most efficient performance in terms of road holding.

$$f_d = \begin{cases} C_{max}(\dot{z}_2 - \dot{z}_1), & if\ \dfrac{\dot{z}_2}{(\dot{z}_2 - \dot{z}_1)} \geq \dfrac{C_{sky}}{C_{max}} \\ C_{sky}\dot{z}_2, & if\ \dfrac{C_{sky}}{C_{max}} > \dfrac{\dot{z}_2}{(\dot{z}_2 - \dot{z}_1)} > \dfrac{C_{sky}}{C_{min}} \\ C_{min}(\dot{z}_2 - \dot{z}_1), & otherwise \end{cases} \quad (1.10)$$

In the study, Cmax and Cmin represent the semi-active damper's maximum and minimum damping coefficients, respectively. Csky is the skyhook damping constant, which is adjusted based on road inputs. $\dot{z}_2$ and $\dot{z}_1$ represent sprung velocities.

The control strategy effectiveness was benchmarked against three distinct skyhook control methods as introduced in the studies by Bessinger et al. (1995) [40] and Nguyen et al. (2009) [41]. The modified skyhook approach developed by Kashemet et al. (2015) [39] demonstrated a notable 38.4% enhancement in ride comfort over passive systems. Meanwhile, Nguyen et al. (2009) [41] observed a 27.3% improvement in their optimal skyhook control method. Additionally, Bessinger et al. (1995) [40] reported a 2.8% increase in performance using their modified skyhook control, and Karnopp et al. (1974) [27] recorded a 5.9% improvement with continuous skyhook control. The modified skyhook system thus stands out for significantly improving ride comfort and outperforming both passive systems and other skyhook variants. Espinoza et al. (2014) [42] further explored this area by investigating three hybrid control strategies for semi-active suspensions: a combination of skyhook and ground hook controls, a hybrid mix-1-sensor approach, and a frequency estimation-based controller.

In commercial magneto-rheological (MR) dampers, an innovative approach involving artificial neural networks (ANN) has been adopted. This system was seamlessly integrated with a controller area network (CAN), utilizing a microcontroller to fine-tune the balance between comfort and road handling efficiency. Compared to conventional solutions, this method

exhibited superior performance as validated through pseudo-Bode diagrams and RMS index analysis.

Model predictive control (MPC), an advanced technique for dynamic system management, is gaining traction due to its proficiency in addressing various process constraints, including cost, safety, and actuator limits. Supported by a wide array of commercial software, MPC allows for extensive customization in model identification, controller design, and performance tuning [43,44]. The core principle of MPC involves the iterative, finite optimization of the system model, a concept depicted in the schematic diagram in Figure 1.1 [45,46,48].

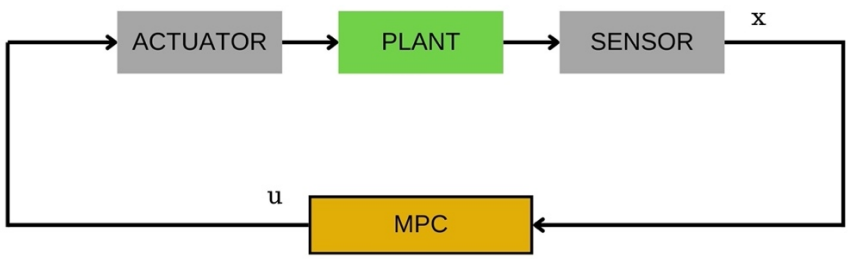

Figure 1.1: Schematic representation of a model predictive algorithm[45]

MPC uses the model to predict the future states of the system and computes the optimal control actions to drive the plant to a reference while considering disturbances and constraints on the control inputs u. Model predictive control uses finite impulse response models and dynamic matrix control [47]. Park et al. (2022) [51] developed a modal controller for an active suspension system using different 1-DOF models for three basic motions (pitch, heave, and roll) of the sprung mass. The modal controller was developed using LQ SOF methodology and a heuristic optimization technique to determine the optimal gain matrix. The frequency analysis and simulations showed that the modal controller design using LQR and SMS was effective in controlling the sprung mass motions and improving ride comfort [52,53

Different control strategies have been proposed for active suspension systems in vehicles. Schmitt et al. [54] used a proportional-integral sliding mode algorithm to control a half car with active suspension robustly. Schubert et al. [55] proposed a control that combines active suspension and ESP to optimize roll angle acceleration and suspension dynamic stroke. Schwenzer et al. [57] studied the effectiveness of a direct drive electromagnetic active suspension system and designed a LQR control strategy to enhance both ride comfort and vehicle stability. Another control proposed by Schwenzer et al. used a finite frequency method to account for actuator input delay and frequency constraints. Serale et al. [58] proposed a set of fuzzy logic controllers to account for actuator delay and faults. MPC controls are widely used due to their robustness, as seen in the MPC-based two-stage hierarchical control presented by Shekhar et al.[60] and the MPC-based trajectory control proposed by Shen et al.[61] to decrease lateral displacements after a burst tire. Wu et al. [62] developed an MPC-based non-linear control, and Xie et al. [63] studied an MPC scheme based on neural networks for non-linear control of the engine throttle and wastegate. Different control strategies have been proposed for vehicle suspensions, including autonomous ground vehicles and hydro-pneumatic suspensions.

Yin et al.[64] investigated a speed tracking control using MPC for precise speed control in autonomous vehicles. Hydro-pneumatic suspensions are commonly used for their high bearing capacity and adjustable non-linear stiffness, and semi-active control can provide improved roll and pitch vibrations [65]. A hybrid control strategy was proposed to control active vehicle roll with electric control and adjustable damping coefficients. Yoon et al. [66] created a device using MR fluid to change the damping behavior of the hydro-pneumatic suspension.

Yu et al. [67] studied a control algorithm for a semi-active suspension system to balance stiffness and prevent end-stop collisions. Luczko and Ferdek [68] introduced a dual-tube

hydraulic damper to optimize the damping force by adjusting pressure differences. Zhang et al.[70] developed a semi-active suspension model using a virtual reference model and a state observer with an Unscented Kalman Filter and SMC controller. Luczko and Ferdek[69] also studied the air spring ECAS vehicle height regulation system and developed a new damper with multiple adjustable levels and an optimized switching sequence for better performance.

Zhongjun et al. [71] presented a particle swarm optimization using a new SMC method to control a semi-active suspension's damping force accurately. Though the overall performance of the semi-active system was better than that of a traditional passive hydro-pneumatic system, the performance was not satisfactory in the low-frequency range. In 2002, Zinober [72] proposed the concept of an inerter for the first time. An inerter can be characterized by the applied force at the two terminals, which is directly proportional to their relative acceleration. Inerters have immense potential at low-frequency levels and have been successfully adapted into mechanical systems such as vehicle suspensions, train suspension, bridge vibration isolation, and for cultural heritage protection. Integrating an inerter in a non-linear energy sink, Zou et al. [73] proposed an effective vibration control system.

Zou et al. [74] optimized a mass-damper-inerter system with tuned Maxwell to reduce bridge vibrations from vortices. Waldrop et al.[75] improved earthquake resistance in statues with a passive vibration isolator and inerter, sparking renewed interest in mechatronic networks. There are various types of inerters, including rack and pinion, ball screw, and fluid-based. Qin et al. [76] introduced a semi-active inerter with force tracking for improved dynamic efficiency and more effective control force tracking. The advantages of semi-active suspension with an inerter have been established and utilized in adaptive vibration absorbers. Wu et al. [77] studied acceleration and velocity-based control methods to optimize the dynamic performance of a

vibration isolator with a semi-active inerter. An active vibration control system with an inerter was also proposed to stabilize the control loop through relative acceleration feedback.

Developing an MPC controller involves three stages: Model predictive control, generalized predictive control, and receding horizon control. Model predictive control uses finite impulse response models and dynamic matrix control [47]. Generalized predictive control models are based on single-input-single-output models used in adaptive control, and receding horizon control is an extension of linear quadratic controllers that aims to minimize the quadratic criteria while ensuring terminal equality constraints [48]. Over time, the differences between these methods have diminished, and the term predictive or model predictive control is now used to describe the same concept [49,50]. Park et al. (2022) [51] developed a modal controller for an active suspension system using different 1-DOF models for three basic motions (pitch, heave, and roll) of the sprung mass. The modal controller was developed using LQ SOF methodology and a heuristic optimization technique to determine the optimal gain matrix. The frequency analysis and simulations showed that the modal controller design using LQR and SMS was effective in controlling the sprung mass motions and improving ride comfort [52,53]

Different control strategies have been proposed for active suspension systems in vehicles. Schmitt et al. [54] used a proportional-integral sliding mode algorithm to control a half car with active suspension robustly. Schubert et al. [55] proposed a control that combines active suspension and ESP to optimize roll angle acceleration and suspension dynamic stroke. Schwenzer et al. [57] studied the effectiveness of a direct drive electromagnetic active suspension system and designed a LQR control strategy to enhance both ride comfort and vehicle stability. Another control proposed by Schwenzer et al. used a finite frequency method to account for actuator input delay and frequency constraints. Serale et al. [58] proposed a set of fuzzy logic controllers to account for actuator delay and faults. MPC controls are widely

used due to their robustness, as seen in the MPC-based two-stage hierarchical control presented by Shekhar et al.[60] and the MPC-based trajectory control proposed by Shen et al.[61] to decrease lateral displacements after a burst tire. Wu et al. [62] developed an MPC-based non-linear control, and Xie et al. [63] studied an MPC scheme based on neural networks for non-linear control of the engine throttle and wastegate. Different control strategies have been proposed for vehicle suspensions, including autonomous ground vehicles and hydro-pneumatic suspensions.

Yin et al.[64] investigated a speed tracking control using MPC for precise speed control in autonomous vehicles. Hydro-pneumatic suspensions are commonly used for their high bearing capacity and adjustable non-linear stiffness, and semi-active control can provide improved roll and pitch vibrations [65]. A hybrid control strategy was proposed to control active vehicle roll with electric control and adjustable damping coefficients. Yoon et al. [66] created a device using MR fluid to change the damping behavior of the hydro-pneumatic suspension.

Yu et al. [67] studied a control algorithm for a semi-active suspension system to balance stiffness and prevent end-stop collisions. Luczko and Ferdek [68] introduced a dual-tube hydraulic damper to optimize the damping force by adjusting pressure differences. Zhang et al.[70] developed a semi-active suspension model using a virtual reference model and a state observer with an Unscented Kalman Filter and SMC controller. Luczko and Ferdek[69] also studied the air spring ECAS vehicle height regulation system. They developed a new damper with multiple adjustable levels and an optimized switching sequence for better performance.

Zhongjun et al. [71] presented a particle swarm optimization based on a new SMC method to control a semi-active suspension's damping force accurately. Though the overall performance of the semi-active system was better than a traditional passive hydro-pneumatic system, the performance was not found to be satisfactory in the low-frequency range. In 2002, Zinober [72]

proposed the concept of an inerter for the first time. An inerter can be characterized by the applied force at the two terminals, which is directly proportional to their relative acceleration. Inerters have immense potential at low-frequency levels and have been successfully adapted into mechanical systems such as vehicle suspensions, train suspension, bridge vibration isolation, and cultural heritage protection. Integrating an inerter in a non-linear energy sink, Zou et al. [73] proposed an effective vibration control system.

Zou et al. [74] optimized a mass-damper-inerter system with tuned Maxwell to reduce bridge vibrations from vortices. Waldrop et al.[75] improved earthquake resistance in statues with a passive vibration isolator and inerter, sparking renewed interest in mechatronic networks. There are various types of inerters, including rack and pinion, ball screw, and fluid-based. Qin et al. [76] introduced a semi-active inerter with force tracking for improved dynamic efficiency and more effective control force tracking. The advantages of semi-active suspension with an inerter have been established and utilized in adaptive vibration absorbers. Wu et al. [77] studied acceleration and velocity-based control methods to optimize the dynamic performance of a vibration isolator with a semi-active inerter. An active vibration control system with an inerter was also proposed to stabilize the control loop through relative acceleration feedback.

Ride Comfort and Road-Handling

The significance of ride comfort in heavy vehicles has been a topic of ongoing research, mainly due to its impact on drivers who often spend extended periods behind the wheel. The interplay between ride comfort and the vehicle's road handling abilities is well-recognized, with the latter having a substantial influence on the former. A deeper understanding of this interplay is necessary to improve ride comfort in these vehicles. Uys et al. (2007) [78] explored the ideal suspension settings to enhance ride comfort in off-road vehicles traversing various road conditions at different speeds, employing the DQ algorithm and ADAMS software. Earlier, Els

and Uys (2003) [79] sought to optimize ride comfort by assessing the root mean square (RMS) value of vertical acceleration at the driver seat under periodic road excitation, using a weighted acceleration approach based on the BS-6841 filter.

Eleberg and Karnoop (1996) [80] delved into the influence of broadband stochastic roadway forces on suspension deflection in a quarter-car model, using power spectral density (PSD) analysis across varying intensities. Their goal was optimal isolation balanced with controlled suspension deflection RMS values. Mastinu and team (2001) [81] developed transfer functions for variables such as the standard deviation of vertical force between the tire and road, vertical body acceleration, and the relative displacement of the wheel to the body. They expanded their analysis to different PSD models, seeking a balance between performance indices. Their findings outlined the optimal settings for suspension damping, stiffness, and tire stiffness, considering variables like speed and specific operational limits. In a related study, Lozia (1991) [82] investigated lateral vehicle dynamics, including factors like acceleration, velocity, displacement, and heading angle. A notable outcome was a 23% reduction in road roughness impact when considering lateral displacement relative to lane width.

In 2004, Marzaband et al. [83] analyzed a coarsely paved road by assessing its elevation spectral density and the standard deviation of surface irregularities, noting a significant lift of 0.01 meters. Their approach involved using a half-car model with four degrees of freedom to ascertain the most favorable suspension settings for enhanced ride comfort. Similarly, Tamboli and Joshi's work in 1991 [84] focused on determining the optimal coefficients for spring damping and stiffness. Their methodology aimed to minimize the vertical acceleration mean square value in vehicles navigating sinusoidal highways and city roads at varying speeds. Kassyzadeh and his team 2014 [85] utilized a quarter-car model categorizing road roughness based on the ISO 2631-1 standard. They employed MATLAB® to simulate the PSD function

of road roughness at steady vehicle speeds, identify critical challenges in suspension vibration, particularly resonance, and maximum adhesion, and explore the effect of tire grip on surfaces.

Further efforts to enhance vehicle comfort have been noted in vehicle dynamics. Kong et al. 2014 [86] conducted experimental simulations on an urban bus, examining its erratic vibrations on dual-track terrains. Their study led to developing a bus frequency model incorporating modal excitation data to streamline computational processes. Ke and Jie 2010 [87] introduced the virtual proving ground (VPG) software, utilizing LS-DYNA to analyze body acceleration across time and frequency spectrums comprehensively. This innovative approach boosts ride comfort, reduces production expenses, and accelerates the development process.

In their 2007 research, Els and colleagues (Els et al., 2007) undertook enhancing the ride comfort of an off-road vehicle. They aimed to achieve this by identifying the optimal settings for dampers and springs tailored to various road profiles and velocities. They further developed these settings into a sophisticated four-stage semi-active hydro-pneumatic suspension system known as 4S4 to expand upon their findings. Subsequently, they applied the DQ algorithm to optimize the Land Rover vehicle, effectively implementing the improved suspension system.

Els, in a prior study from 2005 (Els, 2005) [79], conducted a comprehensive evaluation of ride comfort, utilizing four distinct standards (BS-6841, ISO-2631, AAP, VDI-2057). This assessment involved the analysis of vertical body responses and root mean square (RMS) values. Such a multifaceted approach allowed for a thorough comprehension of a vehicle's ride comfort, serving as a foundation for potential enhancements in the future.

Traditionally, vehicles' endeavors to enhance ride comfort have predominantly revolved around applying linear one-dimensional models [80]. These models, often characterized by limited degrees of freedom and linear elastic-damping components, do not fully capture the non-linear nature of biodynamic response functions. Furthermore, most research efforts have

concentrated on assessing human comfort through vertical vibrations, with scant attention given to transverse vibrations and the impacts of random or quasi-random vibrations and repeated shocks.

In 2004, Yang et al. (2004) [88] delved into ride comfort in railway vehicles. Their approach involved modeling the vehicle as a moving load sequence, incorporating two-degree-of-freedom systems as it traversed simple supported single and three-span bridges. The measure of comfort was primarily based on the maximum acceleration level experienced by passengers. Simultaneously, Lin et al. (2001) [89] established a safety criterion for irregularities in train travel, considering both passenger comfort and safety standards as critical factors in their analysis.

In a related study, Demicd et al. (2002) explored the impact of broadband random road conditions on biodynamic models in road vehicles. Their research, conducted in two phases, initially focused on the influence of these conditions, marking a significant step in understanding the complexities of ride comfort and its correlation with road conditions.

In 2000, Nisihiyam et al. [90] assessed the vibrational characteristics of various vehicle subsystems. These included the vehicle and elements such as the human occupant, seat, steering wheel, and pedals. They subjected these components to both sinusoidal and random excitations. The findings of this study unveiled a noteworthy revelation - the angle of the arm during driving played a pivotal role in influencing the dynamic behavior of humans and the overall comfort experienced during the ride. This groundbreaking insight prompted further exploration into ride comfort within the context of vehicular transportation.

Subsequent research endeavors delved into the intricate relationship between human posture and ride comfort, considering both drivers and passengers. Kargornovin and his team (2005) [91], for instance, investigated the ride comfort of a high-speed train as it traversed a bridge.

They assessed this comfort using metrics such as the Sparling index and the peak value of vertical acceleration.

In 2017, Ataei et al. [92] introduced a novel approach to enhance ride comfort by developing a hybrid electromagnetic suspension system. This innovation was seamlessly integrated with a two-degree-of-freedom (2 DOF) quarter suspension model, showcasing the potential for significant improvements in the overall riding experience.

Furthermore, Mohajer et al. (2017) [93] proposed a technique involving digital filters to modify the frequency weighting factors outlined in ISO 2631 and 5349. Additionally, they introduced a passive three-dimensional (3D) biodynamic model designed to represent the seated occupants of road vehicles. This multifaceted approach aimed to create a more accurate representation of human response to vehicular vibrations.

In 2001, Boileau et al. [94] extensively synthesized existing data. They defined the ranges of DPMI (discomfort perception magnitude index) and STHT (short-term health threshold) characteristics within the frequency range of 0.5x10^20 Hz for vehicle driving. These findings were subsequently incorporated into the ISO-5982 (2001) standard, thus reinforcing their significance in the field.

The following section will shed light on the areas of research that have yet to be explored, drawing upon a comprehensive review of the existing literature. This review will serve as a foundation for identifying gaps in our understanding and guiding future investigations.

1.3 Research Gap

Based on the literature review, several research gaps are identified in the area of ride comfort and vehicle suspension control.

1. The optimization of suspension systems is important for enhancing the ride comfort of a vehicle. However, despite the availability of various methods to improve suspension performance, an optimal suspension system is rare. This is largely due to the influence of suspension settings and road conditions, which can greatly affect the ride comfort of a vehicle.

2. Few studies have attempted to create a ride comfort model that takes into account both the driver's seat and the cabin, as the focus is usually on peak vertical accelerations. A more comprehensive evaluation is necessary to better understand the comfort level experienced by the driver.

3. Although there have been attempts to integrate controllers into suspension systems, the influence of hybrid controllers on the heave of vehicles is not well documented. Further research is necessary in this area as current limited studies indicate the need for more in-depth exploration.

4. The majority of research on ride comfort and road holding is focused on passive suspension integrated systems, leaving room for more exploration in this area. By broadening the scope of research, it is possible to develop a more comprehensive understanding of how suspension systems and road conditions affect the ride comfort and stability of a vehicle.

There has been extensive research on suspension systems, particularly on semi-active and passive systems. Many researchers have examined various semi-active control strategies using practical methods and software such as MATLAB/Simulink®. The skyhook and groundhook control logic hybrid combination has been widely studied, however, other control logic combinations for hybrid control logic have not yet gained popularity.

1.4 Goals of the Project

The goal of the current research work is to create a detailed model for heavy road vehicles that takes into account various factors such as random road excitations, MPC based hook damping control system. The objectives of the research work have been established through a thorough literature review as follows:

i. A mathematical framework of a heavy road vehicle's pitch plane model was found using the Lagrangian approach and was simulated with varying parameters to study its dynamic behavior under random road conditions according to ISO 8608.

ii. To use a control model with hybrid hook damping strategies needs to be developed and integrated with the vehicle's suspension system. The model will be based on a Model Predictive Control (MPC) framework which allows for real-time optimization of control decisions and prediction of future system behavior. Hybrid hook damping strategies refer to a combination of different types of damping mechanisms, such as hydraulic and mechanical damping, to achieve optimal performance.

iii. To conduct ride comfort analysis, the weighted vertical acceleration values need to be calculated and superimposed on ISO 2631 curves for artificial road conditions. This process involves determining the motion of a vehicle or ride system and evaluating the resulting comfort level for the passengers. The ISO 2631 standard provides guidelines for measuring human exposure to whole-body vibration and provides curves for assessing the vibration levels for different applications. The weighted vertical acceleration values help to account for the influence of different frequencies on the human body and can provide a more accurate assessment of ride comfort.

iv. The goal of the research is to compare the effectiveness of Model Predictive Control (MPC) based hybrid hook control strategies against conventional control models in terms of ride comfort and road holding for heavy vehicle systems.

1.5 Project Contribution

This project seeks to study of heavy road vehicle dynamics in the following ways:

Mathematical Modeling through Lagrangian Approach: The previous research has focused primarily on car vehicles rather than heavy vehicles. This project is proposing to use a mathematical model based on Lagrange mechanics to study the truck frame and carry out simulations using random road conditions according to ISO 8608 standards.

MPC based Hybrid Hook Control Framework: The semi-control logics are control systems used to regulate the suspension system of heavy vehicles. In the study, two types of semi-control logics have been modeled using Simulink software: On-off skyhook and continuous skyhook. The simulation results of these two logics are compared in detail to evaluate their performance. Where the two logics are combined to create three different hybrid control logics. A hybrid control logic is a combination of two or more control systems that aim to improve the performance of the suspension system. The study has combined the On-off skyhook and continuous skyhook logics to create three hybrid control logics that can potentially improve the performance of the suspension system. Finally, the hybrid control logic is integrated with a Model Predictive Control (MPC) framework and a Heavy Vehicle Suspension (HVS) model. MPC is a control strategy that uses a mathematical model of the system to predict future behavior and determine the optimal control action. Integrating the hybrid control logic with MPC and HVS suspension model can improve the overall performance and stability of the suspension system.

Ride Comfort and Road Holding: The study conducted a ride comfort analysis for the heavy vehicle system based on the criteria specified in ISO 2631. This standard provides guidelines for evaluating the ride comfort of vehicles. To evaluate the ride comfort of the heavy vehicle system, the Root Mean Square (RMS) weighted value of the vertical accelerations of the Heavy Vehicle Suspension (HVS) integrated with the Model Predictive Control (MPC) model was captured and compared to ISO curves. The RMS value is a measure of the overall magnitude of the vertical accelerations experienced by the vehicle, and the comparison with ISO curves allows for evaluation of the ride comfort based on established standards. Additionally, the study presented a comparison of the ride comfort between a conventional suspension system and a control-based suspension system at different road conditions and speeds. This comparison provides insights into the performance benefits of using a control-based suspension system in improving the ride comfort of heavy vehicles.

1.6 Summary of Project

The project comprehensively investigates heavy road vehicle dynamics, focusing on enhancing ride comfort and road holding by applying model predictive control (MPC) and hybrid hook damping strategies. The summary of the thesis can be outlined as follows:

Chapter 1 serves as an introduction, presenting the objectives, motivation, and literature survey. It establishes the purpose of the research and provides a theoretical background on vehicle modeling, MPC-based control frameworks, ride comfort, and road holding for various vehicle systems.

Chapter 2 details the formulation of the heavy vehicle system (HVS) using the Lagrangian approach. It explains the system's configuration, defines generalized coordinates, and derives the equations of motion through the Lagrange function and variational formulation. The resulting equations are expressed in state space format.

Chapter 3 focuses on applying MPC for the suspension system of heavy vehicles. A hybrid hook damping strategy is proposed, and an MPC-based hybrid hook controller will be integrated with the pitch plane model of a road truck. Simulations are conducted under random road conditions following ISO 8608 standards.

Chapter 4 addresses ride comfort and road-holding criteria based on ISO 2631. The weighted vertical accelerations are analyzed and superimposed over ISO 2631 curves to determine fatigue limits. The impact of the MPC-based control network is compared to that of the conventional system, showcasing the effectiveness of the proposed method. The simulations are carried out using Matlab/Simulink software.

Chapter 5 concludes the thesis by summarizing the essential findings and contributions. It emphasizes the potential for future research in heavy road vehicle dynamics, considering areas identified for further exploration and development.

Chapter 2

Mathematical Modeling of Heavy Road Vehicle through Lagrangian Approach

2.1 Introduction

Several studies have been conducted to analyse the dynamics of vehicles using various mathematical modelling approaches. However, there is a lack of research specifically focusing on road trucks. While the finite element method and modal superposition technique have been widely used to study the dynamic characteristics of road vehicles, most analyses have been limited to specific types of models. Research efforts have predominantly concentrated on studying the effects of railway vehicles on track irregularities leaving a scarcity of studies investigating the behaviour of large road vehicles subjected to arbitrary road conditions. Considering the diverse road conditions in different countries, it becomes challenging for vehicle manufacturers to maintain comfort levels that adhere to ISO standards across all road situations. The suspension system of a vehicle plays a crucial role in ride quality but it faces challenges when encountering various road conditions.

This chapter addresses these gaps by deriving the Lagrange equations for a finite pitch plane model of the heavy vehicle system (HVS) using a lumped mechanic approach. The derived equations are then transformed into a state space representation. Simulations are conducted to visualize the response of the HVS under random road conditions as specified by ISO 8608. These simulations provide insights into the dynamic behaviour of the road truck and its response to different road profiles thus helping to understand the performance of the suspension system.

2.2 Mathematical Modeling for Heavy Vehicle System through Lagrangian Approach

Lagrange equations are highly valuable as they offer reliable techniques for deriving equations of motion for various mechanical systems. One of the key advantages of Lagrange's equations is their versatility, allowing for their application to diverse mechanical systems. Moreover, these equations unveil the intrinsic connection between symmetric properties and the conservation principles of dynamical systems. This insight further enhances the understanding of mechanical systems and their behaviour.

Joseph L. C. Lagrange introduced a comprehensive framework for describing dynamical systems using generalized coordinates. This approach involves considering scalar quantities such as kinetic energy, potential energy and work. The Lagrangian, denoted as L, is defined as the difference between the system kinetic energy and potential energy. This relationship is mathematically expressed as Eq. 2.1.

$$L = T - V \tag{2.1}$$

Here is the L Lagrangian function, T is the total kinetic energy, and V is the total potential energy and neither depends on velocity. For n generalized coordinates, Lagrange's equations of motion can be written as

$$\frac{d}{dt}\left(\frac{\partial L}{\partial \dot{q}_i}\right) - \frac{\partial L}{\partial q_i} = 0,$$

$$\text{for } i = 1 \ldots n. \tag{2.2}$$

Lagrange developed the equations using the virtual work principle, and they only work when the system is considered closed, the constraints are integrable, and there is no gyroscopic coupling.

2.2.1 Mathematical Formulation for Pitch Plane Model

The truck vehicle is considered as a rigid body and its motion is described using a local coordinate reference frame *(t, x)*. The center of mass, denoted as M, is located at the uniformed primary axis of inertia, as illustrated in Figure 2.1. The truck has a pitch inertia, denoted as *J*, with respect to the displacement of the body, $p_1(t)$, and the pitch velocity, $\theta(t)$.

A pitch plane model is employed to describe the suspension system, with the damping coefficient (R_1) and spring stiffness(k_1) representing the damping and spring elements respectively. The vehicle different displacements are defined based on equilibrium positions and are denoted as p (x, t) for vertical deflection and θ(t) for pitch rotation about the transverse horizontal axis [101][104].

Key aspects of the pitch plane model include:

1. Treating the vehicle body components as a rigid body.
2. Considering the suspension damper and spring coefficients as linear features.
3. Using a massless spring damper in the model.
4. Modelling the tire as a spring element, contributing to the overall stiffness.
5. Providing input data for the positions of the spring's two ends, which connect either two rigid bodies or one rigid body and one contact point.
6. Utilizing spring-damper connections to hold the rigid bodies together.
7. Assuming random road inputs and a straight traveling road.

The mathematical formulation of the pitch plane model for the road is based on the Rayleigh beam approach which represents the road as a free-free beam structure. To describe this model,

let's consider the transverse deflection of the chassis as $p_1(t)$. The Lagrangian expression for the truck model can be written as follows [103]:

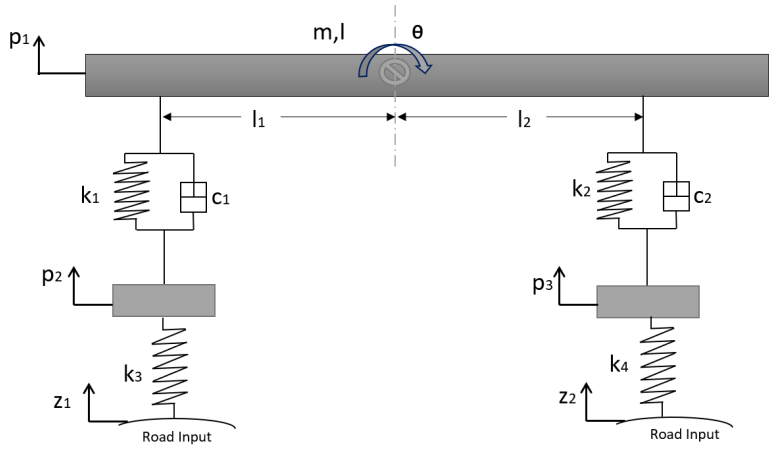

Figure 2.1: *Schematic diagram of a pitch plane model*

$$T = \frac{1}{2}m\dot{p}_1 + I_\theta\dot{\theta} + \frac{1}{2}m_3\dot{p}_3\dot{\theta} + \frac{1}{2}m_2\dot{p}_2 \tag{2.3}$$

$$V = \frac{1}{2}k_2(p_1 - l_2\theta - p_3)^2 + \frac{1}{2}k_1(p_1 + l_1\theta - p_2)^2 + \frac{1}{2}k_3(p_3 - z_3)^2 + \frac{1}{2}k_4(p_2 - z_1)^2 \tag{2.4}$$

$$R = \frac{1}{2}c_2(\dot{p_1} - l_2\dot{\theta} - \dot{p_3})^2 + \frac{1}{2}c_1(\dot{p_1} + l_1\dot{\theta} - \dot{p_2})^2 \tag{2.5}$$

The equations of the motion may be obtained through well-known expressions of variational formalism Equations (2.6-2.9)

$$\frac{\partial}{\partial t}\left(\frac{\partial T}{\partial \dot{p_1}}\right) - \frac{\partial T}{\partial p_1} + \frac{\partial R}{\partial \dot{p_1}} + \frac{\partial V}{\partial p_1} = 0 \tag{2.6}$$

$$\frac{\partial}{\partial t}\left(\frac{\partial T}{\partial \dot{\theta}}\right) - \frac{\partial T}{\partial \theta} + \frac{\partial R}{\partial \dot{\theta}} + \frac{\partial V}{\partial \theta} = 0 \tag{2.7}$$

$$\frac{\partial}{\partial t}\left(\frac{\partial T}{\partial \dot{p_2}}\right) - \frac{\partial T}{\partial p_2} + \frac{\partial R}{\partial \dot{p_2}} + \frac{\partial V}{\partial p_2} = 0 \tag{2.8}$$

$$\frac{\partial}{\partial t}\left(\frac{\partial T}{\partial \dot{p_3}}\right) - \frac{\partial T}{\partial p_3} + \frac{\partial R}{\partial \dot{p_3}} + \frac{\partial V}{\partial p_3} = 0 \tag{2.9}$$

In this case, we are considering z_1, z_2 in the potential energy,

$$m_1\ddot{p}_1 + c_2(\dot{p}_1 - l_2\dot{\theta} - \dot{p_3}) + c_1(\dot{p}_1 + l_1\dot{\theta} - \dot{p_2}) + k_2(p_1 - l_2\theta - p_3)$$

$$+k_1(p_1 + l_2\theta - p_2) = 0 \tag{2.10}$$

$$I\ddot{\theta} + (-c_2 l_2)(\dot{p}_1 - l_2\dot{\theta} - \dot{p}_3) + c_1 l_1(\dot{p}_1 + l_1\dot{\theta} - \dot{p}_2) + (-k_2 l_2)(p_1 - l_2\theta - p_3)$$

$$+\ k_1 l_1(p_1 + l_1\theta - p_2)=0 \tag{2.11}$$

$$m_2\ddot{p}_2 + (-c_2)(\dot{p}_1 + l_1\dot{\theta} - \dot{p}_2) + (-k_1)\left(\dot{p}_1 + l_1\dot{\theta} - \dot{p}_2\right) + k_4(p_2 - z_1) = 0 \tag{2.12}$$

$$m_3\ddot{p}_3 + (-c_2)(\dot{p}_1 - l_2\dot{\theta} - \dot{p}_3) + (-k_2)(p_1 - l_2\theta - p_3) + k_3(p_3 - z_2) = 0 \tag{2.12}$$

Simplified above equations,

$$m_1\ddot{p}_1 = -c_2(\dot{p}_1 - l_2\dot{\theta} - \dot{p}_3) - c_1(\dot{p}_1 + l_1\dot{\theta} - \dot{p}_2) - k_2 D_1 - \ k_1 D_2 \tag{2.13}$$

$$I\ddot{\theta} = (-c_2 l_2)(\dot{p}_1 - l_2\dot{\theta} - \dot{p}_3) + c_1 l_1(\dot{p}_1 + l_1\dot{\theta} - \dot{p}_2) - k_2 l_2 D_1 + k_1 l_1 D_2 \tag{2.14}$$

$$m_2\ddot{p}_2 = (-c_2)(\dot{p}_1 + l_1\dot{\theta} - \dot{p}_2) + (-k_1)D_2 + k_4 D_3 \tag{2.15}$$

$$m_3\ddot{p}_3 = (-c_1)(\dot{p}_1 - l_2\dot{\theta} - \dot{p}_3) + (-k_2)D_1 + k_3 D_4 \tag{2.16}$$

$$D_1 = (p_1 - l_2\theta - p_3) \tag{2.17}$$

$$D_2 = (p_1 + l_1\theta - p_2) \tag{2.18}$$

$$D_3 = p_2 - z_1 \tag{2.19}$$

$$D_4 = p_3 - z_2 \tag{2.20}$$

2.2.2 State Space Representation

The state space form may be represented as,

$$\dot{x}(t) = \mathbf{A}x(t) + \mathbf{B}u(t) \tag{2.21}$$

The state space model of the model can be derived as follows,

$$\dot{x}(t) = \begin{bmatrix} \ddot{p}_1 \\ \ddot{\theta} \\ \ddot{p}_2 \\ \ddot{p}_3 \\ \dot{D}_1 \\ \dot{D}_2 \\ \dot{D}_3 \\ \dot{D}_4 \end{bmatrix}, \qquad x(t) = \begin{bmatrix} \dot{p}_1 \\ \theta \\ \dot{p}_2 \\ \dot{p}_3 \\ D_1 \\ D_2 \\ D_3 \\ D_4 \end{bmatrix}, \quad u(t) = \begin{bmatrix} z_1 \\ z_2 \end{bmatrix}$$

$$\mathbf{A} = \begin{bmatrix} a_{11} & a_{12} & a_{13} & a_{14} & a_{15} & a_{16} & a_{17} & a_{18} \\ a_{21} & a_{22} & a_{23} & a_{24} & a_{25} & a_{26} & a_{27} & a_{28} \\ a_{31} & a_{32} & a_{33} & a_{34} & a_{35} & a_{36} & a_{37} & a_{38} \\ a_{41} & a_{42} & a_{43} & a_{44} & a_{45} & a_{46} & a_{47} & a_{48} \\ a_{51} & a_{52} & a_{53} & a_{54} & a_{55} & a_{56} & a_{57} & a_{58} \\ a_{61} & a_{62} & a_{63} & a_{64} & a_{65} & a_{66} & a_{67} & a_{68} \\ a_{71} & a_{72} & a_{73} & a_{74} & a_{75} & a_{76} & a_{77} & a_{78} \\ a_{81} & a_{82} & a_{83} & a_{84} & a_{85} & a_{86} & a_{87} & a_{88} \end{bmatrix} \qquad \mathbf{B} = \begin{bmatrix} b_{11} & b_{12} \\ b_{21} & b_{22} \\ b_{31} & b_{32} \\ b_{41} & b_{42} \\ b_{51} & b_{52} \\ b_{61} & b_{62} \\ b_{71} & b_{72} \\ b_{81} & b_{82} \end{bmatrix}$$

Whereas,

$a_{11} = -c_2 - c_1$; $a_{12} = c_2 l_2 - c_1 l_1$; $a_{13} = c_1$;

$a_{14} = c_2$; $a_{15} = -k_2$; $a_{16} = -k_1$;

$a_{17} = a_{18} = 0$;

$a_{21} = -c_2 . l_2 + c_1 l_1$ $a_{22} = c_2 l_2^2 + c_1 l_1^2$ $a_{23} = c_1 l_1$

$a_{24} = c_2 l_2$ $a_{25} = -k_2 l_2$ $a_{26} = -k_1 l_1$

$a_{27} = a_{28} = 0$

$a_{31} = -c_2$; $a_{32} = c_2$; $a_{33} = a_{34} = a_{35} = a_{38} = 0$;

$a_{36} = -k_1$; $a_{37} = k_4$;

$a_{41} = -c_1$; $a_{42} = c_1 l_2$; $a_{43} = a_{46} = a_{47} = 0$;

$a_{44} = c_1$ $a_{45} = -k_2$ $a_{48} = k_3$

$a_{51} = 1$; $a_{52} = -l_2$; $a_{53} = a_{56} = a_{57} = a_{58} = 0$;

$a_{54} = -1$

$a_{61} = 1$ $a_{62} = l_1$ $a_{63} = -1$

$a_{64} = a_{65} = a_{66} = a_{67} = a_{68} = 0;$

$a_{73} = 1$ $a_{71} = a_{72} = a_{74} = a_{75} = a_{76} = a_{77} = a_{78} = 0;$

$a_{84} = 1$ $a_{81} = a_{82} = a_{83} = a_{85} = a_{86} = a_{87} = a_{88} = 0;$

$b_{11} = b_{21} = b_{31} = b_{41} = b_{51} = b_{61} = b_{81} = 0;$ $b_{71} = 1;$

$b_{21} = b_{22} = b_{32} = b_{42} = b_{52} = b_{62} = b_{72} = 0;$ $b_{82} = 1;$

The output may be determined as

$$y(t) = \mathbf{C}x(t) + \mathbf{D}u(t) \tag{2.22}$$

2.3 Simulation Study

Studies using simulations are often adaptable and may be changed to account for a situation's changing surroundings. In this simulation work, four types of road inputs (H1, H2, H3 and H4) are simulated which is prescribed by ISO 8608. All simulations are run for 1 sec and simulated on MATLAB/Simulink® software. In simulation work, a total of 1024 records are employed, with an error level maintained at 5.0×10^{-4}. In the current study, the Runge-Kutta Gill technique is applied in the fifth order [102].

2.3.1 Random Road Inputs (ISO 8608)

A random road profile is generated according to the international organization for standardization (ISO 8608). Through an assessment of the PSD of the vertical displacements M_d, as a function of spatial frequency $n(n = \Omega/2\pi(cycles)/m)$ $\mathrm{n}(\mathrm{n} = \Omega/2\pi\,\mathrm{cycles/m})$ and angular spatial frequency as well Ω. The ISO 8608 introduces a classification of spatial frequency based on conventional values of angular spatial frequency $\mathrm{n}_0 = 0.1\,\mathrm{cycles/m}\; cycles/m$ and

spatial frequency $n_0 = 0.1$ cycles/m $cycles/m\Omega_0 = 1$ rad/m. There are four major road classes defined ranging from H1 to H4, based on the values of $M_d(n)$ and $M_d(\Omega)$specified in ISO 8608, as illustrated in Table 2.1 [95].

Table 2.1: ISO 8608 values of $M_d(n_0)$ and $M_d(\Omega_0)$

Road Class	$M_d(n_0)$ (10^{-6} m^3)		$M_d(\Omega_0)$ (10^{-6} m^3)	
	Lower Limit	Upper Limit	Lower Limit	Upper Limit
H1	-	32	-	2
H2	32	128	2	8
H3	128	512	8	32
H4	512	2048	32	128
	$n_0 = 0.1 cycles/m$		$\Omega_0 = 1 cycles/m$	

The following equations can be used to calculate the roughness of a road surface profile using ISO 8608:

$$M_d(n) = M_d(n_0)\left(\frac{n}{n_0}\right)^{-v} \tag{2.41}$$

$$M_d(\Omega) = M_d(\Omega_0)\left(\frac{n}{n_0}\right)^{-v} \tag{2.42}$$

A value of 2 is taken for w, where it represents waviness. A random road input has been developed based on the PSD of vertical displacement M_d as a function of spatial frequency n.

The spatial frequency value inside a frequency band Δn is specified by a dispersed road profile and the value of the PSD function is stated as follows:

$$M_d(n) = \lim_{\Delta n \to 0}\left(\frac{\psi_x^2}{\Delta n}\right) \tag{2.43}$$

The mean square value for the purpose of spatial frequency is indicated by ψ_x^2, which represents the component of the signal for the purpose of spatial frequency n encompassed within the frequency band n. The road profile signal is discretized in this sense and consequently consists of an equally spaced set of elevation points. Here, sampling interval is denoted by B and road profile is given by L. Moreover, the maximum sampling spatial frequency c is $1/\mathrm{B}$, corresponds to the maximum effective sampling spatial frequency ($\mathrm{n_{max}}$) is n_{max}in the frequency domain and discretized spatial frequency values $\mathrm{n_i}$ are equally distributed with an interval of (Δn) (Δn) as $1/\mathrm{L}$. In this way, generic spatial frequency value n_i $\mathrm{n_i}$ can be written as $i.\Delta$ni $\cdot \Delta$n and the discrete form of Eq. (2.43) may be presented as

$$M_d(n) = \frac{\psi_x^2(n_i,\Delta n)}{\Delta n} = \frac{\psi_x^2(i.\Delta n,\Delta n)}{\Delta n} \tag{2.44}$$

where i varying from 0 to N, $\mathrm{N} = \mathrm{n_{max}}/\Delta\mathrm{n}$ as $\frac{n_{max}}{\Delta n}$, using a simple harmonic function, one can calculate the road profile.

$$h(x) = A_i\, cos(\,2\pi.n_i.x + \phi) = A_i\, cos(\,2\pi.i.x.\Delta n + \phi) \tag{2.45}$$

where, amplitude is denoted by $\mathrm{A_i}$, spatial frequency is denoted by $\mathrm{n_i}$ and phase angle is φ. The mean square value can be used to generate harmonic signals.

$$\psi_x^2 = \frac{A_i^2}{2} \tag{2.46}$$

Therefore,

$$M_d(n_i) = \frac{\psi_x^2(n_i)}{\Delta n} = \frac{A_i^2}{2.\Delta n} \tag{2.47}$$

Table 2.2: k values for ISO road roughness classification

Road Class		**k**
Lower Limit	**Upper Limit**	
H_1	H_2	3
H_2	H_3	4
H_3	H_4	5

It has been demonstrated in several investigations that an artificial road profile can only be created using Eq. 2.45 if the PSD function of vertical displacements is well understood, with a random phase angle following a uniform probability distribution in the range of 0 to 2π. The artificial profile can be given as

$$h(x) = \sum_{i=0}^{N} A_i \cos(2\pi . n_i . x + \phi_i) = \sum_{i=0}^{N} \sqrt{2 . \Delta n . M_d(i . \Delta n)} \cdot A_i \cos(2\pi . i . x . \Delta n + \phi) \tag{2.48}$$

Using Eq. (2.47) in Eq. (2.45), a random road profile can be generated according to ISO classification by the following equation.

$$h(x) = \sum_{i=0}^{N} \sqrt{\Delta n .} \cdot 2^k \cdot 10^{-3} \cdot \left(\frac{n_0}{i \cdot \Delta n}\right) \cos(2\pi . i . x . \Delta n + \phi) \tag{2.49}$$

where L = 250, N = 100, and x is the abscissa variable from 0 to L; ; Δn is taken as 1/L; n_{max} is taken as 1/B; and N is $\frac{n_{max}}{\Delta n}$ or L/B; constant is designated as k, depending on the ISO categorization of road profiles. It has also assumed integers augmenting from 3 to 9, which

corresponds to profiles from class H1 to H4 (as shown in Table 2.3); here, k is assumed to take the value 3 corresponding to the class A road profile and $M_d(n_0)$ $\mathrm{G_d(n_0)}$ is taken to be 32, where n_0 is $\mathrm{n_0} = 0.1\,\mathrm{cycles/m}$ $cycles/m$; ϕ_i random phase angle following a uniform probabilistic distribution between 0 to 2π. In this work, four type road conditions (H1-H4) are considered, which are shown in Figures (2.2-2.5).

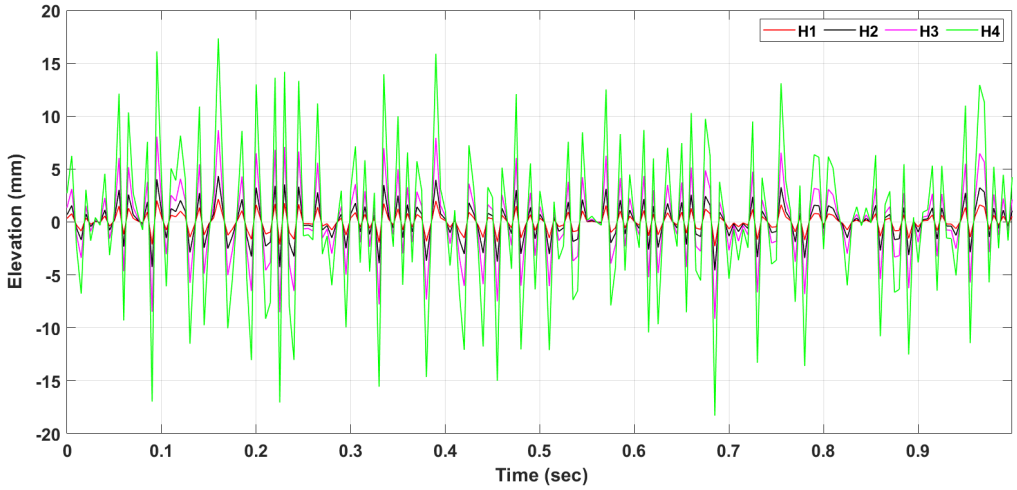

Figure 2.2: *Random road profiles for road categories H1, H2, H3, and H4 at a speed of 40 kilometers per hour.*

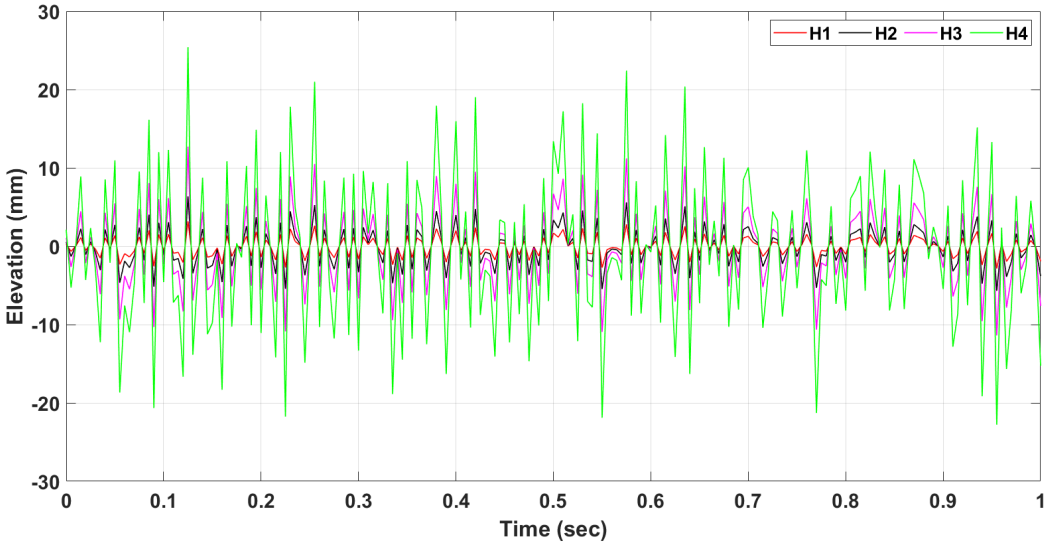

Figure 2.3: *Random road profiles for road categories H1, H2, H3, and H4 at a speed of 60 kilometers per hour.*

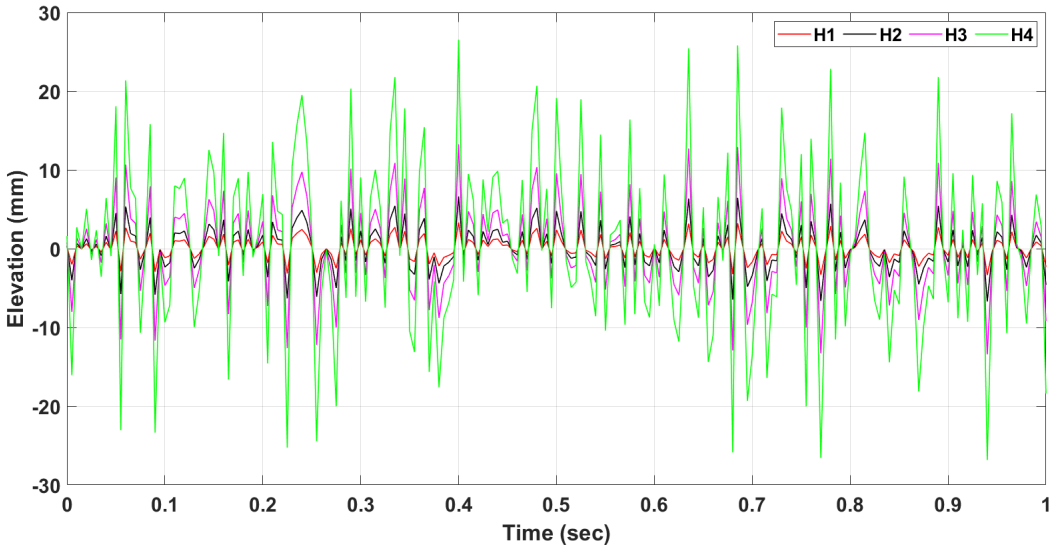

Figure 2.4: *Random road profiles for road categories H1, H2, H3, and H4 at a speed of 80 kilometers per hour.*

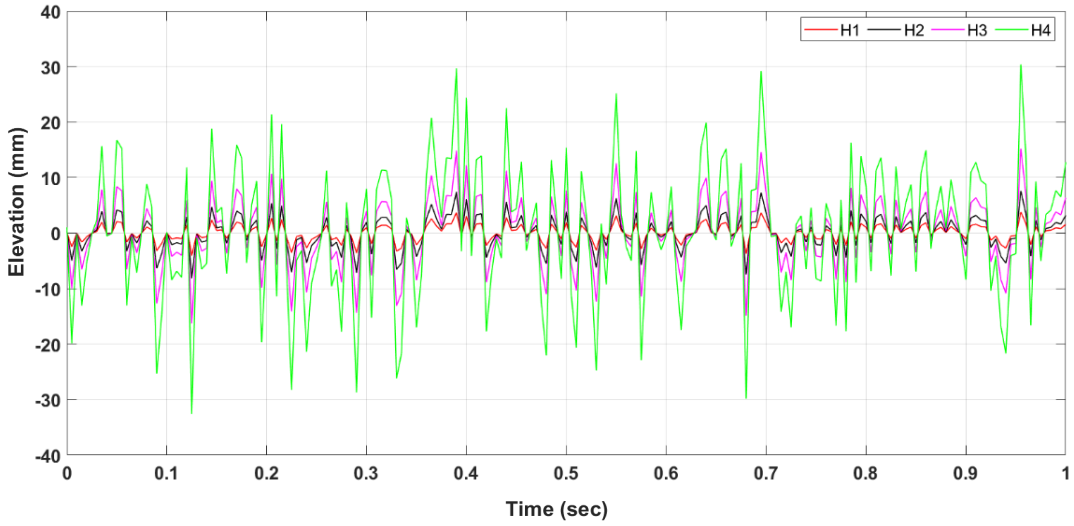

Figure 2.5: *Random road profiles for road categories H1, H2, H3, and H4 at a speed of 100 kilometers per hour.*

The MATLAB/Simulink software is utilized to simulate road profiles based on the ISO 8608 random input mentioned earlier. The simulations encompass various road classifications.

Specifically, road profiles are simulated for four different speeds: 40 km/h, 60 km/h, 80 km/h, and 100 km/h.

In the Figures, the maximum magnitude of the unevenness in the random road profile is depicted. At a speed of 40 km/h, the maximum magnitude is 1.7 cm in an upward direction, while at a speed of 100 km/h, it is -1.8 cm in a downward direction.

Figures 2.2 to 2.5 illustrate the road categories H2, H3, and H4. These figures display the maximum magnitudes of unevenness in the upward direction, which are 2.4 cm, 2.7 cm, and 3 cm, respectively at a speed of 40 km/h. In the downward direction at a speed of 100 km/h, the maximum magnitudes are -2.2 cm, -2.5 cm, and -3.1 cm for H2, H3, and H4 road categories, respectively.

2.4 Conclusions

In this chapter, the focus is on the mathematical modelling of a pitch plane model for a road truck. The model takes into account the presence of two suspension systems that are subjected to random road inputs following the specifications outlined in ISO 8608. Simulations are conducted to visualize the random road inputs for different conditions (H1, H2, H3, and H4) and at various speeds.

The subsequent chapter will delve into the development of a hook damping hybrid control system which utilizes a model predictive control (MPC) system. This control system will be integrated with the pitch plane model of the road truck. Subsequently, the integrated model will be subjected to simulations under different random road response.

Chapter 3

Hybrid Semi-Active Damping Control for Heavy Vehicle Suspension Systems using MPC

In the previous chapter, a mathematical model was established for the pitch plane of a heavy vehicle and simulations were performed to replicate an artificial road condition in accordance with ISO 8608 standards. This chapter delves into the exploration of semi-control techniques and proposes MPC-based hybrid semi-active damping control strategies. The objective is to broaden the scope of vibration reduction methods employed ultimately improving the comfort of heavy vehicles.

3.1 Introduction

Semi-active dampers are divided into two categories; on-off and continuously variable. An on-off damper utilizes a control algorithm to switch between "on" and "off" damping states. The "on-state" damping coefficient is typically high, while the "off-state" damping coefficient is relatively low. However, achieving a damping coefficient of zero in the off-state is not feasible. Conversely, a continuously variable damper adjusts between on and off states, with the on-state damping coefficient modulated to produce varying levels of damping force. Figures 3.1(a) and 3.1(b) illustrate the force-velocity characteristics for on-off and continuous dampers, respectively [32].

The subsequent section provides an overview of various control algorithms used for semi-active damping control such as skyhook, balancing control and groundhook control. Both on-off and continuous versions of these control techniques are discussed [32]. Furthermore, hybrid control strategies that combine multiple control algorithms are explored. The development and

implementation of these control algorithms are demonstrated using half-car models with detailed explanations provided in the following sections [104]

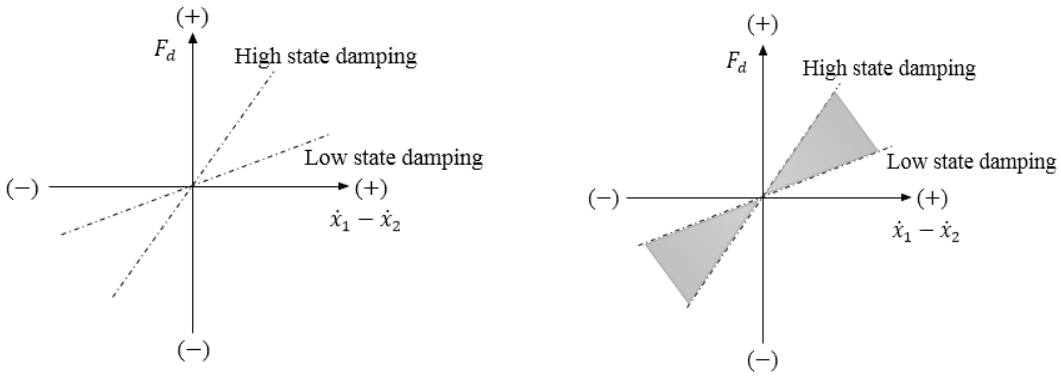

Fig. 3.1: (a) On-off damper, (b) Continuous damper

3.2 Skyhook Control

The skyhook design involves connecting a damper to an inertial reference point in the sky which effectively eliminates the trade-off between resonance control and high-frequency isolation commonly encountered in passive suspensions [96]. Skyhook control primarily targets the motion of the sprung mass reducing it as the skyhook damping coefficient, C_{sky} increases. By isolating the sprung mass from base excitations, skyhook control comes at the cost of increased motion in the unsprung mass. The fundamental algorithm for skyhook control can be summarized as follows:

$$F_d = F_{skyhook} = \begin{cases} c_{sky}\dot{p}_1, & \dot{p}_1(\dot{p}_1 - \dot{p}_2) \geq 0 \\ 0, & \dot{p}_1(\dot{p}_1 - \dot{p}_2) < 0 \end{cases} \tag{3.1}$$

The damping force, F_d, is determined based on the difference between the needed damping force of the skyhook damper, $F_{skyhook}$ and the velocity of the sprung mass, $\dot{p}_1$. This unique configuration effectively addresses the tradeoff commonly encountered in passive suspensions between resonance control and high-frequency isolation. By increasing the skyhook damping coefficient,

c_{sky}, the motion of the sprung mass is reduced. Skyhook control achieves isolation of the sprung mass, $\dot{p}_1$, from base excitations but at the expense of increased motion in the unsprung mass, $\dot{p}_2$.

3.2.1 On-off skyhook control

The on-off skyhook control strategy for the half-vehicle model determines the adjustment of the damper to its maximum or minimum value based on the product of the absolute velocity of the vehicle's sprung mass and the relative velocity across the suspension. In the half-vehicle model depicted in Figure 2.2 (Chapter 2), the absolute velocity of the sprung mass can be calculated as follows:

$$\dot{p}_{abs,f} = \dot{p}_1 - l \cdot \dot{\theta} \tag{3.2}$$

$$\dot{p}_{abs,r} = \dot{p}_1 + l \cdot \dot{\theta} \tag{3.3}$$

The following formulas determine the relative velocity across each suspension,

$$\dot{p}_{rel,f} = \dot{p}_1 - \dot{p}_2 - l \cdot \dot{\theta} \tag{3.4}$$

$$\dot{p}_{rel,r} = \dot{p}_1 - \dot{p}_3 + l \cdot \dot{\theta} \tag{3.5}$$

As a result, the on-off skyhook control approach for a half-vehicle model can be summarized as follows:

Front damper:

$$c_{d,f} = \begin{cases} c_{max,f}, & \dot{p}_{abs,f} \cdot \dot{p}_{rel,f} \geq 0, \\ c_{min,f}, & \dot{p}_{abs,f} \cdot \dot{p}_{rel,f} < 0, \end{cases} \tag{3.6}$$

Rear damper:

$$c_{d,r} = \begin{cases} c_{max,r}, & \dot{p}_{abs,r} \cdot \dot{p}_{rel,r} \geq 0, \\ c_{min,r}, & \dot{p}_{abs,r} \cdot \dot{p}_{rel,r} < 0, \end{cases} \tag{3.7}$$

3.2.2 Continuous Skyhook Control

The continuous skyhook control strategy is an extension of the on-off skyhook control strategy. In the 4-DOF half-vehicle model with a skyhook damper connecting the body to an inertial reference point, the damping force can be expressed as follows;

$$F_{skyhook} = c_{sky} \cdot \dot{p}_{abs,f} \tag{3.8}$$

The continuous skyhook control strategy involves the calculation of the skyhook damping force $F_{skyhook}$ using the skyhook damping coefficient c_{sky} and the absolute velocity of the sprung mass $\dot{p}_{abs,f}$. The continuous skyhook control strategy aims to simulate the skyhook damping force by utilizing a semi-active damper connecting the sprung and unsprung masses. Unlike a passive damper that can only absorb energy, the semi-active damping force and the relative velocity across the damper must satisfy the following inequality:

$$F_{sa} \cdot \dot{p}_{rel,f} \geq 0 \tag{3.9}$$

To create the required force $c_{sky} \cdot \dot{p}_{abs,f}$, it is necessary for $\dot{p}_{abs,f}$ and $\dot{p}_{rel,f}$ to have the same sign. When these two velocities have opposite signs, the semi-active damper can generate a force that is opposite to the desired force. In such cases it is preferable to provide no force at all. Therefore, the semi-active damping coefficient can be determined using the following relationships.

Front damper:

$$c_{d,f} = \begin{cases} c_{sky} \cdot \dot{p}_{abs,f}/\dot{p}_{rel,f}, & \dot{p}_{abs,f} \cdot \dot{p}_{rel,f} \geq 0, \\ 0, & \dot{p}_{abs,f} \cdot \dot{p}_{rel,f} < 0, \end{cases} \tag{3.10}$$

Rear damper:

$$c_{d,r} = \begin{cases} c_{sky} \cdot \dot{p}_{abs,r}/\dot{p}_{rel,r}, & \dot{p}_{abs,r} \cdot \dot{p}_{rel,r} \geq 0, \\ 0, & \dot{p}_{abs,r} \cdot \dot{p}_{rel,r} < 0, \end{cases} \tag{3.11}$$

As per Equation 3.11 when the relative velocity is extremely small, the required damping coefficient increases abruptly and tends towards infinity. However, in practical applications the semi-active damper constant is limited by the physical constraints of the damper, with an upper limit, c_{max}, and a lower limit, c_{min}. The control policy can be summarized as follows, taking into account these limitations:

Front damper:

$$c_{d,f} = \begin{cases} \max\{c_{min,f}, \min[(c_{sky,f} \cdot \dot{p}_{abs,f}/\dot{p}_{rel,f}), c_{max,f}]\}, & \dot{p}_{abs,f} \cdot \dot{p}_{rel,f} \geq 0, \\ c_{min,f}, & \dot{p}_{abs,f} \cdot \dot{p}_{rel,f} < 0, \end{cases} \quad (3.12)$$

Rear damper:

$$c_{d,r} = \begin{cases} \max\{c_{min,r}, \min[(c_{sky,r} \cdot \dot{p}_{abs,r}/\dot{p}_{rel,r}), c_{max,r}]\}, & \dot{p}_{abs,r} \cdot \dot{p}_{rel,r} \geq 0, \\ c_{min,r}, & \dot{p}_{abs,r} \cdot \dot{p}_{rel,r} < 0, \end{cases} \quad (3.13)$$

3.3 Balance Control

The goal of the semi-active control system is to maintain equilibrium between the spring and damping forces when they counteract each other while minimizing the damping force in other circumstances. This approach results in reduced or eliminated force transmission when the damper is active and a slight force increase when it is inactive. This control strategy referred to as "relative control," is centered around managing the relative displacement and velocity between the vehicle body and wheels.

3.3.1 On-Off Balance

In the on-off balancing control strategy, the damping coefficient of the semi-active damper in the half vehicle model is adjusted. This coefficient is switched between high and low values depending on the relative displacement and velocity across the damper. When the product of these two values

is less than or equal to zero, the damper is set to the high state. Conversely, if the product is greater than zero the damper is set to the low state. The relative displacement in the half vehicle model can be determined using the equation presented in Figure 2.1 of Chapter 2.

$$p_{rel,f} = p_1 - p_2 - l \cdot \theta \tag{3.14}$$

$$p_{rel,r} = p_1 - p_3 + l \cdot \theta \tag{3.15}$$

The relative velocity across the damper can be calculated using equations 3.14 and 3.15. This information is used to implement the on-off balancing control logic which determines the state of the damping coefficient.:

Front damper:

$$c_{d,f} = \begin{cases} c_{max,f}, & p_{rel,f} \cdot \dot{p}_{rel,f} \leq 0, \\ c_{min,f}, & p_{rel,f} \cdot \dot{p}_{rel,f} > 0, \end{cases} \tag{3.16}$$

Rear damper:

$$c_{d,r} = \begin{cases} c_{max,r}, & p_{rel,r} \cdot \dot{p}_{rel,r} \leq 0, \\ c_{min,r}, & p_{rel,r} \cdot \dot{p}_{rel,r} > 0, \end{cases} \tag{3.17}$$

3.3.2 Continuous Balance Control

In continuous balancing control for the half vehicle model, the damping coefficient is continuously adjusted according to the relative displacement and velocity across the damper. This allows the semi-active damper to act as a spring with negative stiffness effectively counteracting both the spring and damping forces. The desired force can be expressed using the following equation;

$$F_{sa} = \begin{cases} -k_{s,f} p_{rel,f}, & p_{rel,f} \cdot \dot{p}_{rel,f} \leq 0, \\ 0, & p_{rel,f} \cdot \dot{p}_{rel,f} > 0. \end{cases} \tag{3.18}$$

The damping force is adjusted to match the magnitude of the spring force resulting in zero acceleration. This control technique is responsible for determining the appropriate damping coefficient.

$$c_{d,f} = \begin{cases} \dfrac{-k_{s,f} p_{rel,f}}{\dot{p}_{rel,f}}, & p_{rel,f} \cdot \dot{p}_{rel,f} \leq 0, \\ 0, & p_{rel,f} \cdot \dot{p}_{rel,f} > 0. \end{cases} \tag{3.19}$$

The damping coefficient in Eq. (3.19) approaches infinity for $\dot{p}_{rel,f} \to 0$, which is practically impossible. Based on the damper's physical property, the damping coefficient has a maximum value, c_{max}, and a minimum value, c_{min}, considering physical constraints. The damping coefficient is defined as follows:

Front damper:

$$c_{d,f} = \begin{cases} \max\left[c_{min,f}, min\left[\dfrac{-k_{s,f} p_{rel,f}}{\dot{p}_{rel,f}}, c_{max,f}\right]\right], & p_{rel,f} \cdot \dot{p}_{rel,f} \leq 0, \\ c_{min,f}, & D_{rel,f} \cdot \dot{p}_{rel,f} > 0. \end{cases} \tag{3.20}$$

Rear damper:

$$c_{d,r} = \begin{cases} \max\left[c_{min,r}, min\left[\dfrac{-k_{s,r} p_{rel,r}}{\dot{p}_{rel,r}}, c_{max,r}\right]\right], & p_{rel,r} \cdot \dot{p}_{rel,r} \leq 0, \\ c_{min,r}, & p_{rel,r} \cdot \dot{p}_{rel,r} > 0. \end{cases} \tag{3.21}$$

3.4 Groundhook Control

Groundhook logic aims to minimize dynamic tire forces leading to enhanced vehicle handling and reduced road damage. Similar to the skyhook damper, the groundhook damper is assumed to be connected to a fixed point which in this case is the ground.

$$F_d = F_{groundhook} = \begin{cases} c_{gnd}\dot{p}_2, & -\dot{p}_2(\dot{p}_1 - \dot{p}_2) \geq 0 \\ 0, & -\dot{p}_2(\dot{p}_1 - \dot{p}_2) < 0 \end{cases} \quad (3.22)$$

The equation defines the damping force (F_d) in terms of the required damping force ($F_{groundhook}$) of the groundhook damper and the damping coefficient (c_{gnd}) of the same damper.

3.4.1 On-Off Groundhook Control

The on-off groundhook control strategy for the half vehicle model decides whether the damper should be changed to its highest or lowest value based on the product of the absolute velocity of the unsprung mass and the relative velocity across the suspension. The absolute velocity of the unsprung mass for the half car model depicted in Figure 2.1. (Chapter 2) is provided by $\dot{p}_2$ and $\dot{p}_3$ for front and rear suspensions, respectively. Eqs. (3.12) and (3.13) yield the relative velocities throughout each suspension (3.13). As a result, the on-off skyhook control approach for a half vehicle model is as follows:

Front damper:

$$c_{d,f} = \begin{cases} c_{max,f}, & -\dot{p}_2 \cdot \dot{p}_{rel,f} \geq 0, \\ c_{min,f}, & -\dot{p}_2 \cdot \dot{p}_{rel,f} < 0, \end{cases} \quad (3.23)$$

Rear damper:

$$c_{d,r} = \begin{cases} c_{max,r}, & -\dot{p}_3 \cdot \dot{p}_{rel,r} \geq 0, \\ c_{min,r}, & -\dot{p}_3 \cdot \dot{p}_{rel,r} < 0, \end{cases} \quad (3.24)$$

3.4.2 Continuous Groundhook Control

The 4-DOF half-vehicle model incorporates groundhook dampers that connect the body to a ground inertial reference point. The damping force can be expressed using the following equation:

$$F_{groundhook} = c_{gnd} \cdot \dot{p}_{2,3} \tag{3.25}$$

The equation represents the ground-hook damping force ($F_{groundhook}$), which is determined by the ground-hook damping coefficient (c_{gnd}) and the absolute velocity ($\dot{p}_{2,3}$) of the un-sprung mass. The goal is to replicate this damping force by incorporating a semi-active damper between the sprung and un-sprung masses.

However, due to the limitations of a passive damper that can only absorb energy, the semi-active damping force and the relative velocity across the damper must satisfy the inequality:

$$F_{sa} \cdot \dot{p}_{rel,f} \geq 0 \tag{3.26}$$

It is only when the absolute velocity $\dot{p}_2$ and the relative velocity$\dot{p}_{rel,f}$ have opposite signs that the desired force $c_{gnd} \cdot \dot{p}_2$ can be achieved. If the semi-active damping force and relative velocity have the same sign, the semi-active damper can produce a force opposite to the required force and it is preferable not to apply any force at all. In such cases, the semi-active damping coefficient can be determined using the following relationships.

Front damper:

$$c_{d,f} = \begin{cases} c_{gnd} \cdot \dot{p}_2 / \dot{p}_{rel,f}\,, & -\dot{p}_2 \cdot \dot{p}_{rel,f} \geq 0, \\ 0, & -\dot{p}_2 \cdot \dot{p}_{rel,f} < 0, \end{cases} \tag{3.27}$$

Rear damper:

$$c_{d,r} = \begin{cases} c_{gnd} \cdot \dot{p}_3 / \dot{p}_{rel,r}\,, & -\dot{p}_3 \cdot \dot{p}_{rel,r} \geq 0, \\ 0, & -\dot{p}_3 \cdot \dot{p}_{rel,r} < 0, \end{cases} \tag{3.28}$$

According to Equation 3.28, the required damping coefficient experiences a rapid increase and approaches infinity for extremely small relative velocities. However, the semi-active damper

is constrained by its physical limitations, with an upper limit (c_{max}) and a lower limit (c_{min}). Therefore, the control strategy can be modified as follows:

Front damper:

$$c_{d,f} = \begin{cases} \max\{c_{min,f}, \min[(c_{gnd,f} \cdot \dot{p}_2/\dot{p}_{rel,f}), c_{max,f}]\}, & -\dot{p}_2 \cdot \dot{p}_{rel,f} \geq 0, \\ c_{min,f}, & -\dot{p}_2 \cdot \dot{p}_{rel,f} < 0, \end{cases} \quad (3.29)$$

Rear damper:

$$c_{d,r} = \begin{cases} \max\{c_{min,r}, \min[(c_{gnd,r} \cdot \dot{p}_3/\dot{p}_{rel,r}), c_{max,r}]\}, & -\dot{p}_3 \cdot \dot{p}_{rel,r} \geq 0, \\ c_{min,r}, & -\dot{p}_3 \cdot \dot{p}_{rel,r} < 0, \end{cases} \quad (3.30)$$

3.5 Hybrid Control Strategy

Hybrid control strategies can be created by integrating two or more of the control techniques discussed earlier. These hybrid strategies leverage the strengths of each technique, resulting in enhanced performance in terms of vibration isolation and vehicle handling.

3.5.1 Hybrid Skyhook-Groundhook Control

The purpose of this logic is to minimize both the acceleration of the vehicle body and the dynamic tire force. The body of the vehicle is connected to a hypothetical damper that is attached to an inertial reference point in the sky, while the unsprung mass has a damper connected to a reference point on the ground.

Combining both skyhook and groundhook control techniques yields the control algorithm.

$$W_{hybrid-SH-GH} = \alpha W_{skyhook} + (1-\alpha) W_{groundhook} \quad (3.31)$$

The hybrid controller damping force ($W_{hybrid-SH-GH}$) combines the skyhook damping force ($W_{skyhook}$), groundhook damping force ($W_{groundhook}$), and a weighting factor (α) that

determines the trade-off between comfort and handling. The weighting factor ranges from 0 to 1. The on-off skyhook strategy is employed to control the skyhook damping force while the on-off groundhook logic is utilized to regulate the groundhook force.

3.5.2 Hybrid Skyhook-Balance Control

Hybrid strategies similar to the aforementioned hybrid logic, can be developed by combining two or more control techniques. An example of a hybrid control logic illustrated below can be formed by integrating skyhook and balancing logic.

$$W_{hybrid-SH-B} = \beta W_{skyhook} + (1-\beta) W_{balance} \tag{3.32}$$

where $W_{hybrid-SH-B}$ is the hybrid controller damping force, $W_{balance}$ denotes the balance control force which is influenced by a weighting factor (β) which modifies the degree of skyhook control or balance control. If β is equal to 1, the control will be solely skyhook control while if β is equal to 0, it will be purely balance control. The on-off skyhook and on-off balance control algorithms regulate the skyhook and balance damping forces.

3.5.3 Hybrid Groundhook-Balance Control

The hybrid control technique was created by combining the groundhook and balance control logics.

$$W_{hybrid-GH-B} = \gamma W_{groundhook} + (1-\gamma) W_{balance} \tag{3.33}$$

The hybrid controller damping force denoted as $W_{hybrid-GH-B}$, is determined by the weighting factor γ, which adjusts the extent of groundhook control and balancing control. When γ is set to 1, the control is solely based on groundhook control while a value of 0 represents pure balancing control. The on-off groundhook logic governs the groundhook damping force while the on-off balance logic regulates the balance damping force.

3.5.4 Hybrid Skyhook-Groundhook-Balance Control

By combining all three control techniques, a hybrid control approach is formulated to leverage the advantages of each method. The weighting factors δ and μ determine the contribution of the different control systems as stated below. The on-off balancing logic is employed to govern the system.

$$W_{hybrid-SH-GH-B} = \delta W_{skyhook} - \mu W_{groundhook} + (1 - \delta - \mu) W_{balance} \tag{3.34}$$

3.6 MPC based Hybrid Hook Damping Suspension Control Development

In this section, MPC equipped hybrid hook-damping suspension system has been developed following approach proposed by M.Q Nguyen et al. [98]. Adaptive MPC toolbox are attached with hybrid suspension model, which was presented in Eq 3.34. The state space equation of half car model presented in chapter 2, may also be rewritten as follows:

$$\dot{x(t)} = Ax(t) + B_1 z(t) + B_2 u(t) \tag{3.35}$$

$$y\,(t) = Cx(t) + D_1 z(t) + D_2 u(t) + v(t) \tag{3.36}$$

Here,

$$x(t) = [p_1, \theta, p_{2f,} p_{3r,} \dot{p}_1, \dot{\theta}, \dot{p}_{2f}, \dot{p}_{3r}]$$

$$u(t) = \left[u_f, u_r\right]$$

$$z(t) = [z_{1f}, z_{2r}]$$

$$y(t) = [\ddot{p}_1, \ddot{p}_{2f,} \ddot{p}_{3r}, p_1, p_{2f}, p_{3r}]$$

$x(t)$ is the state vector, $u(t)$ is the control vector, $z(t)$ is the road disturbance vector, and $y(t)$ is the output measurement vectors, $v(t)$ is the measurement noise. The system parameters of

the pitch plane model were determined according to the parameters of the half car model. A, B_1, B_2, C, D_1, D_2 are the matrices of the state space representation.

To address the limited MPC optimization problem, the state equation of the suspension system is presented in Eq 3.35 and Eq 3.36, and it must be developed in discrete time using the zero-hold approach and a sampling time (T_s). The obtained discrete time model may denoted as,

$$x_{k+1} = A_g x_k + B_{1g} z_k + B_{2g} u_k \tag{3.37}$$

$$y_k = C_g x_k + D_{1g} z_k + D_{2g} u_k + v_k \tag{3.38}$$

Here A_g, $B_{1g}, B_{2g}, C_g, D_{1g}, D_{2g}$ are the matrices of the state space representation.

The dissipative conditions for the hybrid semi active damper strategies can be transformed into input constraints. It may be noted that from Eqs (3.32-3.34), it follows that:

$$\begin{aligned} C_{minfr}\dot{p}_{relfr} \le F_{hyfr} \le C_{maxfr}\dot{p}_{relfr} \quad &\text{if} \quad \dot{p}_{relfr} \ge 0 \\ C_{maxfr}\dot{p}_{relfr} \le F_{hyfr} \le C_{minfr}\dot{p}_{relfr} \quad &\text{if} \quad \dot{p}_{relfr} < 0 \end{aligned} \tag{3.39}$$

This dissipative constraint can be recast into:

$$\begin{aligned} C_{minfr}\dot{p}_{relfr} \le\ C_{nomfr}\dot{p}_{relfr} + u_{fr} \le C_{maxfr}\dot{p}_{relfr} \quad &\text{if} \quad \dot{p}_{relfr} \ge 0 \\ C_{maxfr}\dot{p}_{relfr} \le C_{nomfr}\dot{p}_{relfr} + u_{fr} \le C_{minfr}\dot{p}_{relfr} \quad &\text{if} \quad \dot{p}_{relfr} < 0 \end{aligned} \tag{3.40}$$

Here, $C_{nomfr} = \frac{C_{maxfr}+C_{minfr}}{2}$

It results: $$\left|u_{fr}\right| \le \frac{C_{maxfr}-C_{minfr}}{2}\left|\dot{p}_{relfr}\right| \tag{3.41}$$

Actually $\dot{p}_{relfr}$ is a combination of the system state $x(t). i. e.\ \dot{p}_{relfr} = C_{in}\, x$ is an appropriate matrix. Since in the discrete domain, the control input u_k must satisfy the following constraints.

$$M_1\, u_k \le \Gamma_1 x_k \quad \text{if} \quad C_{in}\, x_k \ge 0$$

$$M_2\, u_k \le \Gamma_2 x_k \quad \text{if} \quad C_{in}\, x_k < 0 \tag{3.42}$$

Here, M_1, M_2, Γ_1, Γ_2 are appropriate matrices.

Pitch angle θ and heavy vehicle centre of gravity $\ddot{p}_s$, respectively, can be used to characterize ride comfort and road holding capability in this context. The following may be used to determine the performance

$$H_{comfort} = \int_0^T \ddot{p}_s{}^2(t)\, dt \tag{3.43}$$

$$H_{holding} = \int_0^T \theta^2(t)\, dt \tag{3.44}$$

Nevertheless, the results of the equations contradict the goals. Because of this, a control rule must be created to maximize overall performance by appropriately balancing the requirements of Eqs. (3.43) and (3.44) and accounting for the dissipative limitation that is referenced in Eq (3.42). This allows the hybrid semi-active suspension control problem to be expressed as a limited optimization problem that can be solved within the well-known MPC framework. By designating the N_p as the MPC prediction horizon, the quadratic cost function that follows is defined:

$$J\big(U, N_p, x_{k|k}\big) = \sum_{i=0}^{N_p} (1-\rho)\big(\ddot{p}^5_{k+i|k}\big)^2 + \rho\big(\theta_{k+i|k}\big)^2 \tag{3.45}$$

Here, $\ddot{p}^5_{k+i|k}$, $\theta_{k+i|k}$ refers to the body acceleration and pitch predicted by using the model Eq (3.37), given the initial state $x_{k|k}$

and $U = \begin{bmatrix} u_{k|k} \\ u_{k+1|k} \\ \vdots \\ u_{k+N_p-1/k} \end{bmatrix}$, here U is the vector of the control modes to be optimized. $\rho \in [0\ 1]$ is a weighting coefficient that may be adjusted to strike an appropriate balance between handling performance and comfort. The load transfer ratio (LTR) approach can be used to tune

ρ [97][98][99]. The vehicle's LTR may be measured as it is moving and weight is transferred from the front to the back or vice versa, indicating that the vehicle is experiencing pitch motion. By defining the vertical forces acting on the left and right sides by F_{sf} and F_{sr} respectively. It is represented as follows.

$$\begin{cases} F_{sf} = m_s \frac{g}{2} + m_s h \frac{\ddot{p}}{l} \\ F_{sr} = m_s \frac{g}{2} - m_s h \frac{\ddot{p}}{l} \end{cases} \tag{3.46}$$

That allows us to introduce the LTR as:

$$\rho = \left| \frac{F_{sf} - F_{sr}}{F_{sf} + F_{sr}} \right| \tag{3.47}$$

Here $\ddot{p}$ is the longitudinal acceleration of the vehicle at COG. According to Eq 3.46, the LTR ratio can be evaluated online through the measurement of the longitudinal acceleration $\ddot{p}$. Since $\rho \in [0\ 1]$, when $\rho \to 0$, there is neither longitudinal load transfer nor pitch motion which may be minimizes the body acceleration. On another hand, when $\rho \to 1$, the vehicle is within a critical situation caused by the pitch motion.

The optimization problem of the MPC design can be defined as:

$$\min_U J(U, N_p, x_k)$$

$$\text{Subject to} \begin{cases} x_{k+1} = A_g x_k + B_{1g} z_k + B_{2g} u_k \\ M_1\, u_k \le \Gamma_1 x_k \quad \text{if} \quad C_{in}\, x_k \ge 0 \\ M_2\, u_k \le \Gamma_2 x_k \quad \text{if} \quad C_{in}\, x_k < 0 \end{cases} \tag{3.48}$$

Evaluating the cost function as specified in Eq (3.45) is the first step in computing the control action in the MPC framework. Equation 3.37–3.38 provides the state equation that is used for this evaluation, which takes place along the state trajectory inside the prediction horizon. A deviation from the methodology in chapter 2 should be noted when discussing the role of road disturbances. Thus, an extended state observer is developed in order to account for the effects of disturbances during the prediction stage. This observer allows the simultaneous estimate of

the state variables and the road input while taking into account conventional sensors that are already installed.. By using the complete state equation for both state estimate and prediction, this dual estimation is made possible. It is a typical assumption in MPC design that the road disturbance will remain constant during the course of the prediction horizon. i.e. $w_{k+i} = w_k, i = 0 \ldots, N_p - 1$. Now here, the augmented value of state space model presented in Eq 3.35 can be written as,

$$\begin{bmatrix} x_{k+1} \\ z_{k+1} \end{bmatrix} = \begin{bmatrix} A_g & B_{1g} \\ 0 & I \end{bmatrix} \begin{bmatrix} x_k \\ z_k \end{bmatrix} + \begin{bmatrix} B_{2g} \\ 0 \end{bmatrix} u_k \tag{3.49}$$

Now optimization can be written as,

$$\min_U J(U, N_p, x_k)$$

$$\text{Subject to} \begin{cases} \begin{bmatrix} x_{k+1} \\ z_{k+1} \end{bmatrix} = \begin{bmatrix} A_g & B_{1g} \\ 0 & I \end{bmatrix} \begin{bmatrix} x_k \\ z_k \end{bmatrix} + \begin{bmatrix} B_{2g} \\ 0 \end{bmatrix} u_k \\ M_1\, u_k \leq \Gamma_1 x_k \quad \text{if} \quad C_{in}\, x_k \geq 0 \\ M_2\, u_k \leq \Gamma_2 x_k \quad \text{if} \quad C_{in}\, x_k < 0 \end{cases} \tag{3.50}$$

Then, using the receding horizon technique, the MPC control law is calculated, with the actual control action : $u_k = u_{k|k.}$ being limited to the first element in the computed optimum sequence U: However, the dissipative limitation shown in Eq. 3.42 is contingent upon the suspension deflection speed's sign $C_{in}x_k$. Consequently, it is necessary to satisfy the switching between the constraints based on the sign of $C_{in}x_k$. This goal can be achieved by formulating the optimization using a quadratic problem with logic constraints. As a result, integer quadratic programming (MIQP) is combined with the optimization process [98].

To begin creating an observer methodology, the output equation might be expanded in the manner shown below:

$$y_k = [C_d \quad D_{1g}] \begin{bmatrix} x_k \\ z_k \end{bmatrix} + \begin{bmatrix} D_{2g} \\ 0 \end{bmatrix} u_k + v_k \tag{3.51}$$

If the observability of the Eq 3.50 and Eq 3.51 is satisfied. Then the both the system state and road disturbance can be evaluated with following expression:

$$\begin{bmatrix}\hat{x}_{k+1}\\ \hat{z}_{k+1}\end{bmatrix} = A_v\begin{bmatrix}\hat{x}_k\\ \hat{z}_k\end{bmatrix} + B_{2v}u_k + M(y_k - \hat{y}_k) \tag{3.52}$$

$$y_k = C_v\begin{bmatrix}\hat{x}_k\\ \hat{z}_k\end{bmatrix} + \begin{bmatrix}D_{2g}\\ 0\end{bmatrix}u_k$$

Here, *M* is the observer gain that will be designed

$$\text{And } A_v = \begin{bmatrix}A_g & B_{1g}\\ 0 & I\end{bmatrix}, B_{2v} = \begin{bmatrix}B_{2g}\\ 0\end{bmatrix} C_v = [C_g \quad D_{1g}]$$

Let us define the estimation error of the augmented system:

$$e_k = \begin{bmatrix}x_k\\ z_k\end{bmatrix} - \begin{bmatrix}\hat{x}_k\\ \hat{z}_k\end{bmatrix}$$

Then the estimation error can be inferred form Eq (3.49) and Eq. (3.52) as:

$$e_{k+1} = A_v\left(\begin{bmatrix}x_k\\ z_k\end{bmatrix} - \begin{bmatrix}\hat{x}_k\\ \hat{z}_k\end{bmatrix}\right) - LC_v\left(\begin{bmatrix}x_k\\ z_k\end{bmatrix} - \begin{bmatrix}\hat{x}_k\\ \hat{z}_k\end{bmatrix}\right) - Lv_k \tag{3.53}$$

Finally we can simplify this equation,

$$e_{k+1} = (A_v - LC_v)e_k - Lv_k \tag{3.54}$$

The state observer is presented in Eq. 3.52. due to presence of this observer, the robust MPC design can be adopted to the state estimation error presented in Eq. 3.54. The Simulink model is constructed in Figure 3.2 based on above mentioned MPC model.

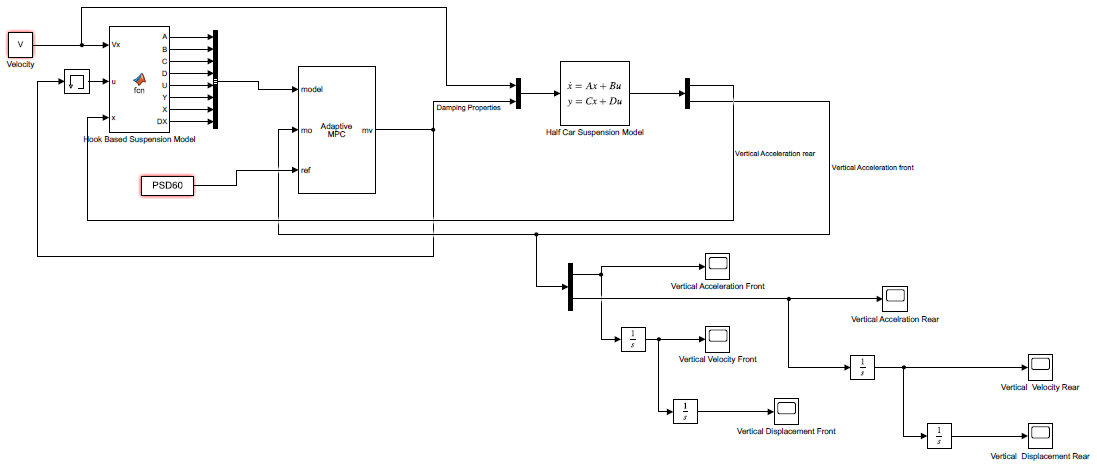

Fig. 3.2: MPC based hybrid hook Simulink model

3.7 Numerical Simulation

Computer simulation offers the advantage of assessing system performance over extended durations in a short amount of computational time. Simulation models are flexible and can be adjusted to simulate dynamic real-world conditions. Differential equations are frequently employed to construct simulation models as the complexity increases. In this study, MATLAB/Simulink® software is utilized to analyse half-car suspension systems under different road profiles and speeds [104].

3.7.1 Parameters of Half Vehicle Model

Table 3.2 displays the simulation parameters for the 4-DOF half vehicle model. In this work, the parameters utilized by Goncalves [96] for a whole automobile model are applied. In the half-vehicle model, the sprung mass and pitch moment of inertia of the complete automobile model from [96] have been halved, but the parameters for the front and rear suspension remain unchanged.

Table 3.1: Model Parameter for 4-DOF half vehicle model [96]

Parameter	Value	Parameter	Value
M_s	730 kg	$c_{max,f}$	2838 Ns/m
$M_{u,f}$	40 kg	$c_{sky,f}$	1290 Ns/m
$M_{u,r}$	35.5 kg	$c_{gnd,f}$	1290 Ns/m
I_{yy}	1230 kg.m^2	$c_{min,r}$	324 Ns/m
$k_{s,f}$	19960 N/m	$c_{max,r}$	3564 Ns/m
$k_{s,r}$	17500 N/m	$c_{sky,r}$	1620 Ns/m
$k_{t,f}$	175500 N/m	$c_{gnd,r}$	1620 Ns/m
$k_{t,r}$	175500 N/m	d_a	1.011 m

$c_{min,f}$	258 Ns/m	d_b	1.803 m

3.8 Results and Discussion

As mentioned earlier, a half-car model was exposed to random road inputs and simulations were performed using the quarter car model Simulink model within the MATLAB/Simulink® software environment. The simulation results were categorized into three groups: i) on-off control strategies, ii) continuous control techniques and iii) hybrid control strategies.

3.8.1 Performance of On-Off Control Strategies

In this section of study, we conduct a thorough evaluation of different on-off semi-active control algorithms and compare their performance. Our primary focus is on two key performance metrics: body acceleration and displacement. These metrics serve as essential indicators of how effective these control strategies are in mitigating vibrations and improving the overall quality of the ride experience.

To provide a visual representation of our findings, we have included Figure 3.3, which illustrates the comparison of body acceleration over time for two main scenarios; the passive suspension system and various on-off semi-active suspension strategies. These simulations were conducted under specific conditions, specifically at a speed of 60 kilometers per hour (km/h) and on a road characterized by H1-based random road conditions.

Our analysis of the results consistently reveals that the semi-active skyhook logic consistently outperforms the passive system. This means that the body acceleration experienced by the

vehicle occupants is notably reduced when utilizing the semi-active skyhook control strategy throughout the experimental duration.

However, it is important to note that the on-off skyhook control strategy exhibits a distinct behaviour. In this approach, the damping force experiences sudden and dramatic changes each time the control function shifts direction. These abrupt transitions lead to the formation of sharp peaks and unexpected jerking motions. Figure 3.3 visually highlights the presence of a substantial number of these abrupt changes. Consequently, while the skyhook method reduces body acceleration compared to the passive system, it introduces a significant amount of discomfort due to these abrupt shifts.

In contrast, the on-off balance control strategy shows a more favourable performance profile. It yields lower body acceleration values with the maximum magnitude remaining below 1-meter per second squared (m/s^2). Additionally, the acceleration values generated by this approach remain consistently lower over a duration of 10 seconds. Furthermore, the on-off balance control strategy results in fewer and less severe jerking motions when compared to the skyhook method, making it a more appealing choice for enhancing ride quality.

In summary, our comprehensive comparison of on-off semi-active control algorithms suggests that the semi-active skyhook logic effectively reduces body acceleration but introduces abrupt transitions. On the other hand, the on-off balance control strategy minimizes body acceleration, maintains lower values consistently and offers a smoother ride experience making it a promising choice for improving overall ride quality.

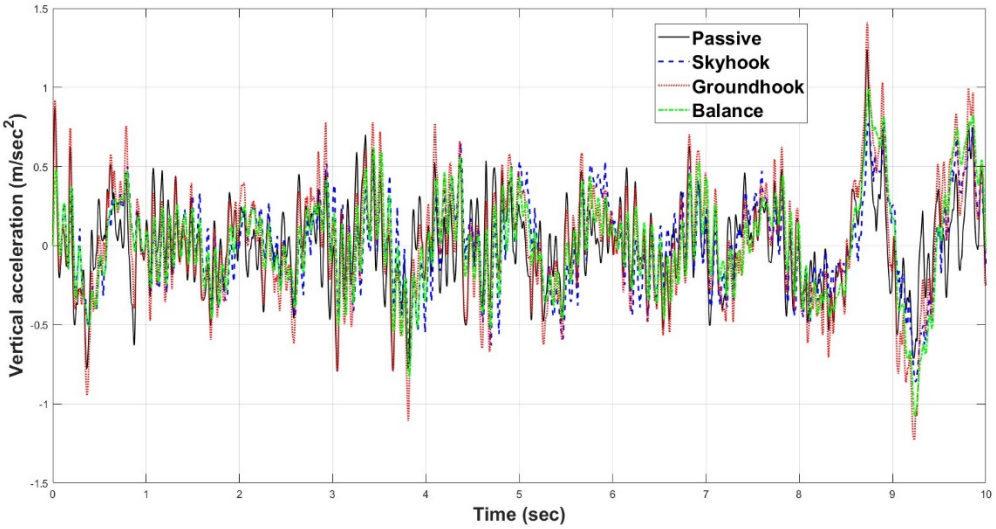

Fig. 3.3: Body acceleration response of on-off control strategies for random input at 60 kmph

3.8.2 Performance of Continuous Control Strategies

We assessed the performance of vehicle models employing continuous control techniques by subjecting them to simulations with random road inputs at a speed of 60 kilometers per hour (kmph). In Figure 3.4, we present the acceleration response of the continuous skyhook control strategy when exposed to random road inputs. Notably, the continuous skyhook control consistently yields lower acceleration values when compared to the passive system throughout the simulation. Furthermore, it is worth highlighting that, in contrast to the on-off skyhook logic, the continuous control approach mitigates the severity of jerking motions, resulting in a smoother ride experience even on uneven terrain. This observation suggests that continuous skyhook control is effective at reducing both body acceleration and the discomfort associated with abrupt movements as we see a lower acceleration amplitude.

Another noteworthy finding is that all three continuous control strategies exhibit greater displacement responses than the passive system. This implies that the vehicle experiences

larger magnitudes of displacement throughout the simulation when continuous control techniques are employed. However, it is important to note that the behaviour of these three continuous control methods closely resembles that of the passive system.

In particular, the continuous skyhook logic stands out as it consistently demonstrates slightly better results over time when compared to the other two continuous control methods. This suggests that continuous skyhook control strikes a favourable balance between minimizing body acceleration and optimizing ride comfort, making it a promising choice for enhancing vehicle performance on uneven road surfaces.

In summary, our evaluation of continuous control techniques in vehicle models, as illustrated in Figure 3.4, highlights the superiority of continuous skyhook control in reducing acceleration and minimizing jerking motions. While all continuous control methods result in greater displacement compared to the passive system, the continuous skyhook approach emerges as a particularly effective solution, offering improved performance while closely resembling the behaviour of the passive system.

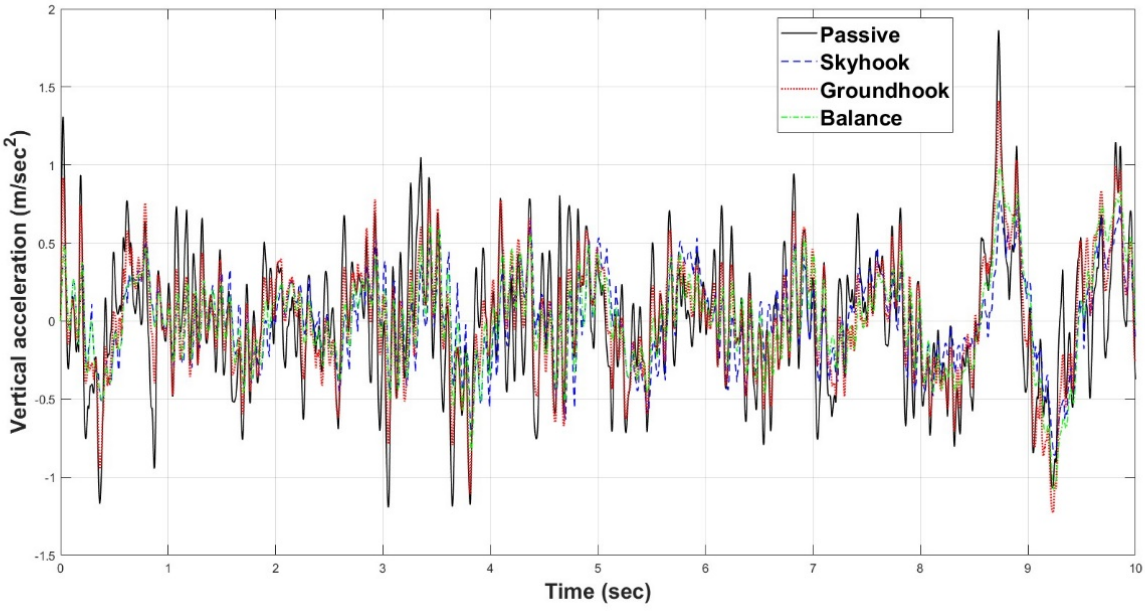

Fig 3.4: Body acceleration response of continuous control strategies for random input at 60 kmph

3.8.3 Performance of Hybrid Control Strategies

In this section, the performance of a semi-active suspension system for a half car was assessed by analysing four hybrid control systems.

When analysing the effects of random road inputs on half of the vehicle, we observed that the HY-SH-GH logic performs similarly to the on-off skyhook logic in some scenarios. However, in other instances it manages to achieve lower acceleration values. Nevertheless, sharp jerking motions persist throughout the simulation. This suggests that while there is similarity between the two systems in certain conditions, the HY-SH-GH logic offers a slight advantage in reducing acceleration.

Now, let us turn our attention to the HY-SH-B logic system which is designed to control a vehicle's acceleration response. Figure 3.5 illustrates the system response to a set of inputs. Notably, the HY-SH-B logic system exhibits a more gradual and smoother acceleration response compared to a passive system. This smoother profile leads to a reduction in acceleration magnitude and a decrease in the occurrence of abrupt peaks. These outcomes underscore the effectiveness of the HY-SH-B logic system in delivering a more comfortable and less jarring driving experience for vehicle occupants.

On the other hand, we have the HY-GH-B logic system, also designed to regulate a vehicle acceleration response. Based on the provided description, it can be inferred that this system's reaction to random road inputs closely resembles that of a passive system. However, the presence of noticeable jerks in the system's response indicates a lack of smoothness. Furthermore, the degree of acceleration varies across different cases with some instances exhibiting higher acceleration while others show lower values. This inconsistency suggests that

the HY-GH-B system fails to provide a uniform acceleration experience, resulting in an unpredictable and less comfortable ride for vehicle occupants.

In summary, the HY-GH-B logic system displays inconsistent behaviour when exposed to random road inputs, characterized by noticeable jerks and varying degrees of acceleration. While its performance aligns with that of a passive system, the higher variation in its response diminishes its effectiveness in delivering a smooth driving experience. In contrast, the HY-SH-GH-B control system demonstrates a reduction in acceleration amplitude compared to the passive system. It exhibits similar strength and frequency of jerking motions as observed in the HY-SH-GH control, indicating comparable acceleration responses for half of the vehicle on a random road.

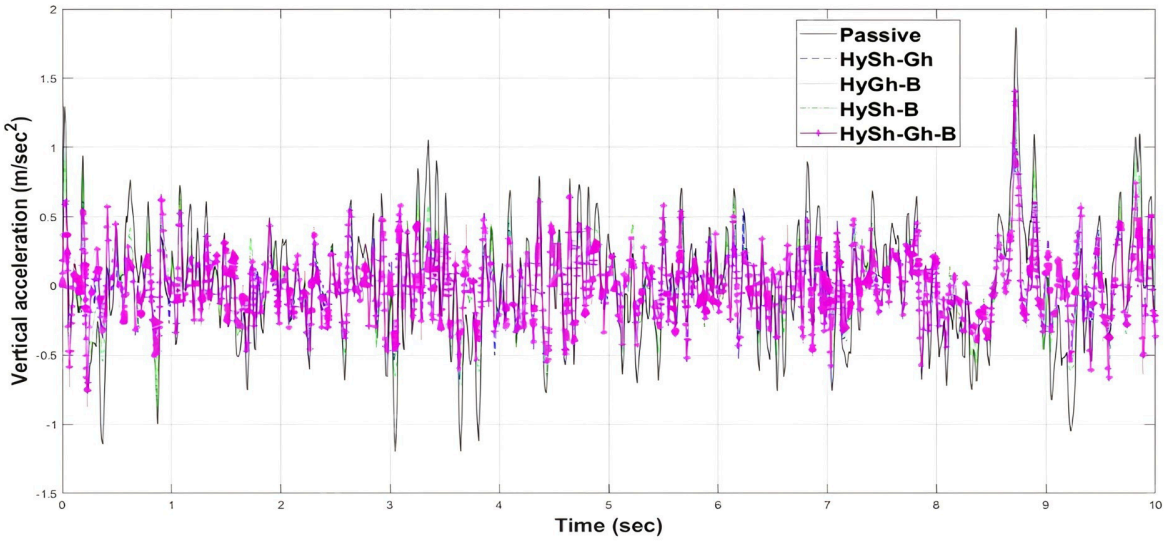

Fig 3.5: Body acceleration response of hybrid control strategies for random input at 60 kmph

3.8.3 Performance of MPC based Hybrid Control Strategies

In the study on the semi-active suspension system for the half-car model, a comprehensive evaluation was conducted on four hybrid control systems and an MPC-based hook control system. The objective was to compare their performance in terms of body acceleration. The

results were analysed and presented in the form of a graph depicting body acceleration versus time, as shown in Figure 3.6.

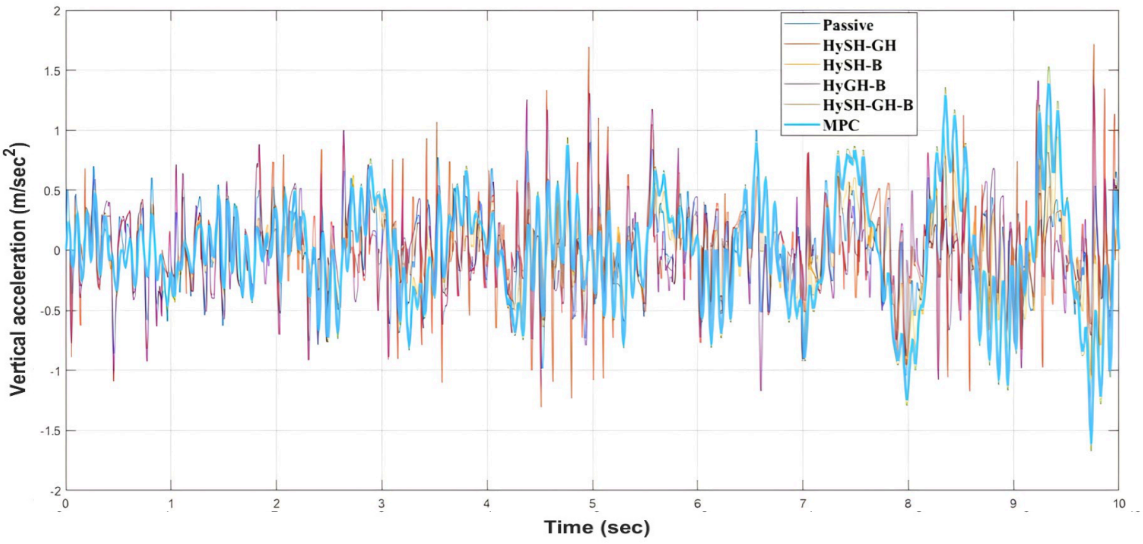

Fig. 3.6: Body acceleration response of MPC based hook suspension system over random input

Remarkably, the MPC-based hook control system outperformed not only the hybrid control systems but also the passive system in terms of body acceleration by reducing the RMS of the best performing hybrid (HY-SH-GH-B) by roughly 25% as we can see lower acceleration amplitudes even if it follows the same pattern. It demonstrated superior performance, indicating its capability to provide a smoother and more comfortable ride experience for the occupants of the half-car model.

These findings highlight the effectiveness of the MPC-based hook control system and certain hybrid control strategies in reducing the vertical acceleration of the half-car model, enhancing ride comfort, and improving the overall performance of the semi-active suspension system.

3.9 Conclusions

The chapter described a control framework for the suspension system in a pitch plane model supported by two suspension systems, subjected to random road input as prescribed by ISO 8608. The chapter carried out simulations to present the random road inputs for different control and hybrid control schemes as well as MPC-based hybrid control. The next chapter will evaluate the ride comfort and road holding of a heavy vehicle system under random road conditions according to the guidelines outlined in ISO 2631. This assessment will provide insights into the performance of the suspension system in maintaining stability and comfort for passengers in real-world conditions.

Chapter 4

Evaluation of Ride Comfort and Road Holding of a Half-Vehicle System with MPC under Random Road Conditions

In the previous chapter, we explored the model predictive control (MPC) based hook damping suspension system for heavy road vehicles. The system was formulated and analysed to understand its dynamic behaviour. In this chapter, our objective is to assess the ride comfort and road holding performance of heavy road vehicles according to ISO 2631 standards.

ISO 2631 is an internationally recognized standard that provides guidelines for evaluating ride comfort in transportation systems. It quantifies the level of vibrations experienced by individuals while traveling in a vehicle. To evaluate ride comfort, we measure the vertical acceleration in a half-car model using ride index weighing functions. These functions are then compared to ISO 2631 curves to determine the level of ride comfort experienced by passengers.

Additionally, we also assess the road holding capability of heavy road vehicles in this chapter. Road holding capability refers to the vehicle's ability to maintain stability and control on different road conditions. This evaluation is crucial to ensure passenger safety and prevent accidents.

We conduct tests and evaluations on the MPC-based hook damping suspension control system to understand its impact on ride comfort and road holding. The results reveal the improvements achieved in the ride comfort and road holding ability of heavy road vehicles with the implementation of the proposed control system.

4.1 Introduction

With increasing industrial demand, overloading and unpredictable road conditions, truck vibration issues have become more prominent in recent years. In the context of large road transportation systems ensuring ride comfort is of utmost importance as drivers spend a significant amount of time in their cabins. Various factors contribute to travel comfort and sedentary activities such as temperature, noise, vibration, seat characteristics, posture and backrest among others. Among these factors, vibration is widely recognized as a critical element of the physical environment that can lead to driver discomfort.

Extensive research on ride comfort emphasizes the significance of addressing vibrations, considering them as one of the primary factors affecting driver well-being. This recognition stems from the understanding that vibrations can significantly impact the overall comfort experience during travel.

4.2 Evaluation of Ride Comfort in Road Vehicle Applications

Ride comfort encompasses both psychological and physiological aspects, and it is evaluated through various techniques that assess the mechanical environment experienced by passengers. To measure human ride comfort, four commonly used approaches are employed: ISO 2631 (Europe), BS 6841 (UK), VDI 2057 (Germany and Austria) and average absorbed power (USA). In the subsequent sections, we will provide a brief overview of these protocols.

4.2.1 AAP (Average Absorb Power)

The average absorbed power (AAP) method, devised by the US Army Tank Automotive Command (Pradko, 1966), is a technique used to assess human comfort in relation to vibrations. This method is based on the elastic characteristics of the human body, which generate restorative forces in response to vibrations resulting in the generation of energy that needs to be absorbed or

dissipated. The absorbed power refers to the rate at which this energy is absorbed (Pradko, 1966). The evaluation process involves analysing ride comfort in both time and frequency domains, providing a comprehensive understanding of the vibrations and motions experienced by drivers or passengers.

$$\text{AP} = \sum_{i=0}^{N} K_i \ (A_{i_{rms}})^2 \tag{4.1}$$

The average absorbed power (AAP) method can be assessed in both time and frequency domains and it exhibits a primary resonance at approximately 4-5 Hz. However, its effectiveness diminishes in the frequency range of 1 to 80 Hz.

4.2.2 BS 6841

The BS 6841 standard is a ride comfort evaluation method specifically designed for road vehicles. It considers a frequency range of 0.5 to 80 Hz and does not rely on time-dependent curves. Instead, it employs the concept of vibration dose value (VDV). The accelerations are weighted using various weighting functions based on different directions. The weighted signal is then utilized to calculate the root mean square (RMS) value, which serves as a measure of ride comfort. Unlike time-based curves, this method emphasizes the importance of weighing the accelerations in the evaluation process.

$$\text{RMS} = \sqrt{\frac{1}{N} . \sum_{n=1}^{N} a_n^2} \tag{4.2}$$

The RMS values of vibration are compared to subjective values to estimate the probable human reaction to vibration. The frequency range may be extended to compensate for motion smoothness based on measurements. The overall ride comfort is evaluated by additional vehicle tests on the same road at the same speed and can be compared directly to other values.

4.2.3 VDI-2057

The first calculation of ride comfort was done using the VDI-2057 standard, published in 1963 by the Society of German Engineers. The standard evaluated comfort by exposing individuals to sine-wave vibrations with specific intensity and frequency and then determining a ride comfort index (K-factor). The K-factor was compared to a subjective table to assess comfort according to human perception. In 1979, the VDI adopted the ISO-2631 tolerance curves while still using the K-factor for subjective comparison to human response. To evaluate the performance, the acceleration response was transformed into the frequency domain using fast Fourier transform (FFT). The RMS values were then calculated at specific third-octave center frequencies and represented as a single value. The weighted RMS acceleration data and K-values in the z-direction are then determined accordingly

$$1 \leq f \leq 4 \text{ Hz} \qquad K_Z = 10.\, a_Z.\, \sqrt{f} \tag{4.3}$$

$$4 \leq f \leq 8 \text{ Hz} \qquad K_Z = 20.\, a_{Z,} \tag{4.4}$$

$$8 \leq f \leq 80 \text{ Hz} \qquad K_Z = 160 a_Z.\, \sqrt{f} \tag{4.5}$$

After the weighted RMS acceleration data and K-values in the z-direction are determined, the weighted signal is plotted using limit plots. The limit plots used are based on those approved by ISO-2631. The frequency range of the bandwidth or the range of frequencies used to measure the vibration is between 1 Hz and 80 Hz. This means that the weighted signals are plotted using data that is collected within this frequency range. This range was chosen as it is considered to provide a comprehensive assessment of the ride comfort, taking into account the different frequencies that contribute to the overall vibration experienced by the occupants.

4.3 Comfort Guidelines -ISO 2631 (*ISO*-2631, 1997)

The ISO 2631 standard outlines a methodology for measuring whole-body vibrations including periodic, random and transient vibrations. The standard outlines key elements that establish the acceptable degree of vibration exposure and offers recommendations for evaluating its potential effect on health, comfort and likelihood of motion sickness. The ISO 2631 standard serves as a reference for engineers and researchers to determine the acceptable limits of vibration exposure in various scenarios and applications.

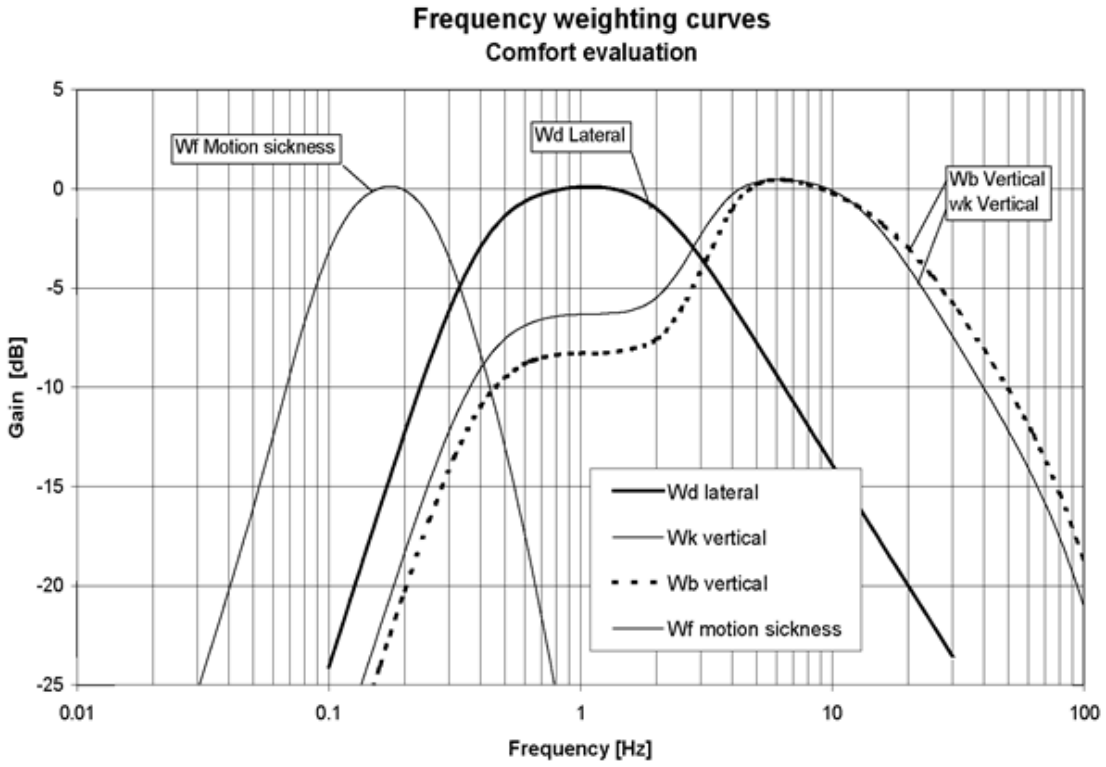

Fig 4.1: *Frequency weighing curves for comfort evaluation*

Table 4.1: Principal frequency weighting in one third octave

Frequency f, ***Hz***	$\mathbf{W}_k$		$\mathbf{W}_d$		$\mathbf{W}_f$	
	Factor ×1000	**dB**	**Factor ×1000**	**dB**	**Factor ×1000**	**dB**
0.1	31.2	-30.11	62.4	-24.09	695	-3.16
0.125	48.6	-26.26	97.3	-20.24	895	-0.96

0.16	79	-22.05	158	-16.01	1006	0.05
0.2	121	-18.33	243	-12.28	992	-0.07
0.25	182	-14.81	365	-8.75	854	-1.37
0.315	263	-11.60	530	-5.52	619	-4.17
0.4	352	-9.07	713	-2.94	384	-8.31
0.5	418	-7.57	853	-1.38	224	-13.00
0.63	459	-6.77	944	-0.50	116	-18.69
0.8	477	-6.43	992	-0.70	53	-25.51
1	482	-6.33	1011	0.10	23.5	-32.57
1.25	484	-6.29	1008	0.07		
1.6	494	-6.12	968	-0.28		
2	531	-5.49	890	-1.01		
2.5	631	-4.01	776	-2.20		
3.15	804	-1.90	642	3.85		
4	967	-0.29	512	-5.82		
5	1039	0.33	409	-7.76		
6.3	1054	0.46	323	-9.81		
8	1036	0.31	253	-11.3		
10	988	-0.10	21	-13.91		
12.5	902	-0.89	161	-15.87		
16	768	-2.28	125	-18.03		
20	636	-3.93	100	-19.90		
25	513	-5.80	80.0	-21.94		
30.1	405	-7.86	63.2	-23.98		
40	314	-10.05	49.4	-26.13		
50	246	-12.19	38.8	-28.22		
63	186	-14.61	29.5	-30.60		
80	132	-17.56	21.1	-33.53		

The ISO 2631 standard addresses vibrations transmitted through supporting surfaces which are commonly experienced in various applications such as vehicles, machines and structures. The

standard defines different frequency ranges for health, comfort, perception and motion sickness. For health, comfort and perception the frequency range is from 0.5 Hz to 80 Hz, while for motion sickness it is from 0.1 Hz to 0.5 Hz.

To evaluate these vibrations, the ISO 2631 standard utilizes RMS values of frequency-weighted accelerations. Translational vibrations are measured in m/s², while rotational vibrations are measured in rad/s². The standard applies weighting curves (Wd for horizontal and Wk/Wb for vertical) to express the weighted RMS acceleration. In railway applications, Wb is used for vertical acceleration. These weighting curves are provided in Figure 4.1 of the ISO 2631 standard.

To calculate the weighted RMS acceleration, the standard provides an equation or its equivalent in the frequency domain, which should be followed for accurate assessments.

$$a_w = \left[\frac{1}{T} \int_0^T \left(a_{wi}(t) \right)^2 dt \right]^{0.5} \tag{4.6}$$

The equation for calculating a_{wi} frequency-weighted acceleration, expressed in m/sec2, takes into account the integration time (T) for the running average and time (t).

The evaluation of the acceleration signal can be performed using either a constant bandwidth or a proportional bandwidth spectrum of unweighted acceleration. The proportional bandwidth method involves dividing the frequency range into one-third octave bands and calculating the weighted RMS acceleration by weighting and summing the data from each one-third octave band. The specific weightings for each band can be found in Table 4.1. The overall weighted acceleration is then determined using an equation in the frequency domain.

$$a_w = \left[\sum_i \left(a_i w_i \right)^2 \right]^{\frac{1}{2}} \tag{4.7}$$

The frequency-weighted RMS acceleration (aw) is obtained by multiplying the RMS acceleration (ai) of each one-third octave band by its corresponding weighting factor (wi), and then summing the results. The acceptable levels of acceleration magnitude for comfort can vary depending on various factors and are not explicitly defined in ISO 2631. However, Table 4.2 serves as a general reference for assessing the expected human response to vibration in public transportation based on the frequency-weighted RMS acceleration values.

Table 4.2: ISO classification of comfort levels

Subjective Comment	**Accelerations value (m/s^2)**
Not Uncomfortable	<0.0315 m/sec^2
A Little uncomfortable	0.0315 to 0.63 m/sec^2
Fairly uncomfortable	0.5 to 1.0 m/sec^2
Uncomfortable	0.8 to1.6 m/sec^2
Very uncomfortable	1.25 to 2.5 m/sec^2
Extremely uncomfortable	>2.0 m/sec^2

4.4 Ride Comfort Guidelines (ISO-2631 approved)

The assessment of ride comfort involves evaluating the human body response to vibration. It is not only influenced by biomechanical and physiological factors but also by environmental factors such as heat, pressure and ventilation. The international standards organization (ISO 2631, 1997) has established limits for human exposure to vibrations in the frequency range from 1-80 Hz which can cause fatigue, discomfort and other health issues if

exposed to frequently. Whole-body vibrations from road vehicles can also cause damage to the back and other health consequences.

Discomfort refers to feelings caused by vibration and can be affected by various factors in different contexts. A limiting value for discomfort should be identified for specific applications. According to ISO, exposure to vibrations within the frequency range of 0.5 Hz to 80 Hz can lead to various health issues such as fatigue, discomfort, obesity and other severe consequences (Griffin, 2012). Prolonged exposure to vibrations transmitted from road vehicles through the seat to the body particularly the pelvis, can result in serious damage to the back and other health issues. Whole-body vibrations also produce diverse and complex sensations that change based on frequency, axis and other variables.

It is important to note that many factors can contribute to the level of discomfort and therefore a specific limiting value for discomfort should be identified for different applications based on the specific needs and requirements. This limiting value should take into account the various factors that can influence discomfort levels. Additionally, different limiting values for discomfort may be appropriate in different contexts, so it is crucial to be aware of these variations when assessing ride comfort in transportation systems.

Figure 4.2 shows that the vertical RMS (root mean square) accelerations at different control configurations in one-third octave bands. The accelerations are superimposed on ISO curves for reduced comfort boundaries over 2.5 hours, 4 hours, and 8 hours. According to the data, the acceleration response of the vehicle body is below the 4-hour curve at 60 km/hr on H1 road conditions. However, for vehicle vibrations the fatigue limit increases up to 8 hours. This means that if a driver is exposed to ride vibrations for more than 4 hours at speeds greater than 60 km/h on H1 road conditions, they may experience a normal or common sense of discomfort.

The figure also indicates that the MPC based suspension system provides more comfort compared to other hybrid strategies as we can see that the RMS weighted acceleration at different frequencies is lower than the other hybrid systems.

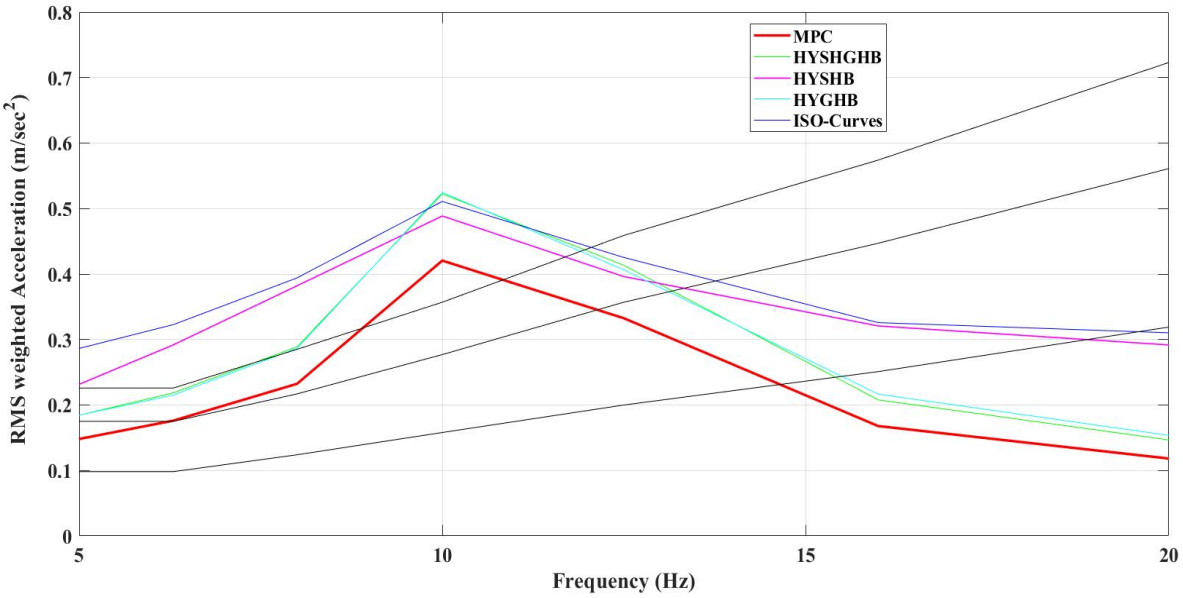

Fig 4.2: Comparison for ride comfort of MPC based suspension with hybrid hook strategies

4.5 Conclusions

The chapter evaluates the ride comfort and road holding of a heavy vehicle system (HVS) on different road conditions. The assessment is performed by measuring the vertical RMS acceleration of a half car model with ride index weighing functions. These measurements are then compared to the ISO 2631 comfort guidelines by superimposing the results over the ISO 2631 curves for reduced comfort boundaries of 2.5 hours, 4 hours, and 8 hours. The chapter concludes by suggesting that the MPC-based suspension system provides a more comfortable ride compared to other hybrid strategies. The next chapter will present the overall conclusions and future scope of the research.

Chapter 5
Conclusions and Future Scope

This dissertation aimed to investigate the dynamic behaviour of a semi-active suspension system designed for heavy vehicles operating under random road conditions, following the guidelines outlined in ISO 8608. The analysis was conducted using simulation techniques, considering both the quarter automobile model and the half car model. Various road profiles including bump-type road profiles and random road inputs, were used to assess the system's performance. The study focused on evaluating different control logics employed in semi-active suspension control and the obtained results are presented and discussed in the following sections.

5.1 Conclusions

1. The dynamic model of a road vehicle was developed using the bond graph approach and implemented in the MATLAB/Simulink® environment.
2. The research focused on a 4-DOF half automobile model to study the behaviour of the system. The tire velocity input was calculated considering half sine bumps and random road irregularities.
3. The primary objective of the study was to analyse the dynamic behaviour of a semi-active suspension system specifically designed for road vehicles. MATLAB/Simulink® was employed to evaluate the system parameters and the performance of various control logics utilized in semi-active suspension control. The analysis was conducted using the half car model subjected to bump-type road profiles and random road inputs. The study encompassed the following aspects of the suspension system: - Vertical acceleration of both the sprung and unsprung masses. - Transmission of acceleration from the wheel to the vehicle body.

4. The on-off skyhook logic exhibited promising results in reducing the vertical acceleration of the body for bump-type inputs. However, it occasionally resulted in sudden jerks and an uncomfortable ride experience. Conversely, the on-off groundhook logic demonstrated improved performance in reducing the acceleration of the unsprung mass leading to quicker dampening of wheel vibration and enhanced road holding force.
5. The study evaluated the performance of different control logics employed in the semi-active suspension system for road vehicles. The results indicated that continuous control logics effectively reduced body acceleration but exhibited longer settling times compared to other control methods. While the continuous control logics successfully minimized body acceleration they took more time to achieve a stable state. Among the hybrid logics, the HY-SH-GH and HY-SH-GH-B demonstrated superior performance in terms of reducing vertical acceleration, resulting in reduced magnitude and severity.
6. Integration of MPC with a combined hybrid model yielded significantly improved results compared to other proposed strategies.
7. Ride comfort assessment was conducted by evaluating the weighting values of vertical acceleration using 1/3-octave band frequencies and overlaying them with ISO 2631 curves.
8. Performance analysis revealed that the MPC-based hook damping suspension system outperformed other hybrid control strategies in terms of overall performance.

5.2 Future scope

The study evaluated the performance of a semi-active suspension system for road vehicles using the bond graph approach and MATLAB/Simulink®. The results of the study suggest several avenues for future research.

- Full car model evaluation: In future studies, the semi-active suspension system can be evaluated using a full car model. This will provide a more complete understanding of the suspension system and its behaviour in a real-world scenario.
- Lateral dynamics: The current study only evaluated the vertical and longitudinal (pitch) dynamics of the suspension system. Future studies can extend the analysis to include the lateral dynamics of the vehicle model.
- Different road inputs: The study used bump type road profile and random road inputs to evaluate the performance of the suspension system. In future studies, other types of road inputs can be considered to provide a more comprehensive understanding of the suspension system behaviour.
- Active suspension system: The study focused on the semi-active suspension system. Future studies can extend the analysis to include active suspension systems with various control strategies. This will provide a comparison of the performance of different suspension systems and control methods.

Overall, the results of the study suggest several avenues for future research to further improve our understanding of suspension systems for road vehicles.

References

1. Demicd, M., Lukicd, J. (2002). Some aspects of the investigation of random vibration influence on ride comfort. *Journal of Sound and vibration,* 253(1), 109-129.
2. Espinoza, A. A. O., Ortega, A. M. C., Martinez, J. C. T., Alcantara, D. H., Menendez, R. M. (2014). Analysis of On/Off controllers of a semi-active suspension in a CAN. *19th IFAC World Congress, Cape Town, South Africa. Aug 24-29, 2014,* 10902-10907.
3. Kim, J.H., Yim, H.J. (1994). Influence of chassis flexibility on dynamic behavior of engine mount systems. *SAE Paper*, 942269.
4. Raj R., A., Shrivastava, S., Trikhande, M. W., (2015). Modelling and analysis of skyhook and fuzzy logic controls in semi-active suspension system. *International Conference on Industrial Instrumentation and Control (ICIC), College of Engineering Pune, India*.
5. Bakar, S.A.A., Samin, P.M., Jamaluddin, H., Rahman, R.A., Sulaiman, S. (2015). Semi active suspension system performance under random road profile excitations. *International Conference on Computer, Communication, and Control technology, April 21-23, Sarawak, Malaysia.*
6. Yoon. I., Hac, A. (1995). Semi active suspension with adaptive capability. *Journal of Sound and vibration,* 180(3), 475-492.
7. Guglielmino, E., Sireteanu, T., Stammers, C. W., Ghita, G., Giuclea, M., (2008). Semi-active suspension control- improved vehicle ride and road friendliness. *Springer-Verlag London Limited.*
8. Parsons, K. C., Griffin, M. J., (1988). Whole-body vibration perception thresholds. *Journal of Sound and vibration.* 121(2), 237-258.
9. Patil, M. K, Palanichamy, M.S., Ghista, D.N., (1977). Dynamic response of human body seated on a tractor and effectiveness of suspension systems. *SAE 770932*, 755-792.

10. Margolis, D., Edeal, D. (1990). Towards an understanding of beaming in large trucks. *Journal of commercial vehicles*, 99(2), 952-959.
11. Margolis, D., Edeal, D. (1989), Modelling and control of large flexible frame vehicles using bondgraphs. *Journal of commercial vehicles*, 98(2), 605-611.
12. Ibrahim, I.M. (1995). Effect of frame flexibility on the ride vibration of heavy truck. *Journal of Computers and Structures,* 58(4), 709-713.
13. Carlbom, P. (2001) Combining MBS with FEM for rail vehicle dynamics analysis. *Multi-body System Dynamics,* 6(3), 291-300.
14. Carlbom, P. (2000). Carbody in rail vehicle dynamics. *PhD Thesis, Stockholm.*
15. Carlbom, P. (2000). Carbody and passengers in rail vehicle dynamics" *PhD Thesis, Royal Institute of Technology, Sweden.*
16. Mukherjee, A. (2001). The issue of invariants of motion for general class of symmetric systems through bondgraph and umbra-Lagrangian. *Proc. of Int. Conf. of Bondgraph Modelling and Simulation* ICBGM'01, 33(1), 295-304.
17. Margolis, D., Shim, T. (2001). A bondgraph model incorporating sensors, actuators, and vehicle dynamics for developing controllers for vehicle safety. *Journal of the Franklin Institute*, 338 (1), 21-34.
18. Li, Lin & Sandu, Corina. (2006). Algorithm for the prediction of traction performance of terrain vehicles. *American Society of Mechanical Engineers, Design Engineering Division (Publication) DE.* 10.1115/IMECE2006-13968..
19. Cao, C. (2005). Approaches to reduce truck beaming. *Society of Automotive Engineers, SAE Paper* 2005-01-0829.
20. Kiencke, U. and Dai, A. (2007). Observation of lateral vehicle dynamics. *Control Engineering Practice,* 5(8), 1145-1150.

21. Fischer, D., M. Börner, J Schmitt, Isermann, R. (2007). Fault detection for lateral and vertical vehicle dynamics. *Control Engineering Practice,* 15 (3), 315–24.
22. Teng, T. L, Chang, F., Liu, Y.S., Peng, C.P., (2008). Analysis of dynamic response of vehicle occupant in frontal crash using multi-body dynamics method. *Mathematical and Computer Modelling,* 48 (11-12), 1724–36.
23. Zhou, J., Goodall, A., Ren, L., Zhang, H. (2009). Influences of car body vertical flexibility on ride quality of passenger railway vehicles. *Part F: Journal. Rail and Rapid Transit,* 2009, 223.
24. Huang Cai-hong, Zeng J. (2010). Flexural vibration suppression of car body for high-speed passenger car based on constrained damping layers, *Journal of Traffic and Transportation Engineering.* 2010 (1), 36-42.
25. Tomioka, T., Takigami T., Aida, K., (2017). Experimental investigations on the damping effect due to passengers on flexural vibrations of railway vehicle car body and basic studies on the mimicry of the effect with simple substitution. *Vehicle System Dynamics,* 55(7), 995-1011.
26. Dumitriu M., Craciun, C., (2017), Modelling of structural flexibility of the railway vehicles car body, *MATEC Web of Conferences*, 07007, 112.
27. Karnopp, D. C., Crosby, M. J., Harwood, R. A., (1974). Vibration control using semi-active force generators. *Journal of Engineering for Industry*, 96 (2), 619-626.
28. Karnopp, Dean & Rosenberg, Ronald & Perelson, Alan. (1976). System Dynamics: A Unified Approach. Systems, *Man and Cybernetics, IEEE Transactions on.* 6. 724-724. 10.1109/TSMC.1976.4309434.
29. Karnopp, D. C., (1990). Design principles for vibration control systems using semi-active dampers. *Journal of Dynamic Systems, Measurement, and Control,* 112,448-455.

30. Alanoly, J., Sankar, S. (1988). Semi-active force generators for shock isolation. *Journal of Sound and Vibration,* 126 (1), 145-156.
31. Alanoly, J., Sankar, S. (1987). A new concept in semi-active vibration isolation. *Journal of Mechanisms, Transmission, and Automation in Design (ASME),* 109(2), 242-247.
32. Liu, Y., Waters, T. P., Brennan, M. J., (2005). A comparison of semi-active damping control strategies for vibration isolation of harmonic disturbances. *Journal of Sound and Vibration* 280(1-2), 21-39.
33. Shamsi, A., Choupani, N., (2008). Continuous and discontinuous shock absorber control through skyhook strategy in semi-active suspension system (4-DOF model), *International Journal of Mechanical, Aerospace, Industrial, Mechatronic and Manufacturing Engineering,* 2(5), 697-701.
34. Strecker, Z., Mazůrek, I., Roupec, J., Klapka, M., (2015). Influence of MR damper response time on semi-active suspension control efficiency, *Meccanica,* 50(8), 1949-1959.
35. Hailong, Z., Enrong, W., Fuhong, M., Rakheja, S., Chunyi, S., (2013). Skyhook-based semi-active control of full-vehicle suspension with magneto-rheological dampers. *Chinese Journal of Mechanical Engineering,* 26(3), 498-505.
36. Amin, M. H. I. M., Hudha, K., Kadir, Z. A., Amer, N. H. (2015). Skyhook control for 7 DOF ride model of armored vehicle due to road disturbance. Paper presented in *ASCC, 10th Asian IEEE.*
37. Raj R., A., Shrivastava, S., Trikhande, M. W., (2015). Modelling and analysis of skyhook and fuzzy logic controls in semi-active Suspension System. *International Conference on Industrial Instrumentation and Control (ICIC), College of Engineering Pune, India.*
38. Strydom, A., Els, P.S., (2014). The applicability of hybrid control to a small off-Road vehicle without a differential, *Proceedings of ASME, International Design Engineering*

Technical Conferences & Computers and Information in Engineering Conference (IDETC/CIE), August 17-20, 2014, Buffalo, New York.

39. Kashem, S. B. A., Ektesabi, M., Nagarajah, R. (2015). Comparison between different sets of suspension parameters and introduction of new modified skyhook control strategy incorporating varying road condition. *Vehicle System Dynamics,* 50(7), 1173-1190.
40. Bessinger, F. H., Cebon, D., Cole, D. J. (1995). Force control of a semi-active damper. *Journal of Vehicle System Dynamics*. 24(9), 695–723.
41. Nguyen, Q. H., Choi, S. B. (2009). Optimal design of MR shock absorber and application to vehicle suspension. *Smart Materials Structure*, 18(3), 035012.
42. Espinoza, A. A. O., Ortega, A. M. C., Martinez, J. C. T., Alcantara, D. H., Menendez, R. M. (2014). Analysis of On/Off controllers of a semi-active suspension in a CAN. *19th IFAC World Congress, Cape Town, South Africa. Aug 24-29, 2014, 10902-10907.*
43. Garc´ıa CE, Prett DM, Morari M (1989) Model predictive control: theory and practice—a survey. *Automatica* 25(3):335– 348.
44. Camacho EF, Bordons C (2004) Model predictive control. *Advanced textbooks in control and signal processing. Springer, London and New York.*
45. Yang Shi, Kunwu Zhang, (2021) Advanced model predictive control framework for autonomous intelligent mechatronic systems: A tutorial overview and perspectives, *Annual Reviews in Control,* Volume 52,170-196.
46. ISSN 1367-5788,Schubert P, Stemmler S, Abel D (2019) Towards predictive anti-sway control of hanging loads: model-based controller design for a knuckle boom crane. *In: 2019 18th European Control Conference (ECC), IEEE, Naples, Italy,* 2276–2282,.
47. Prasad GM, Kedia V, Rao AS (2020) Multi-model predictive control (MMPC) for non-linear systems with time delay: an experimental investigation. *In: 2020 First IEEE*

International Conference on Measurement, Instrumentation, Control and Automation (ICMICA), IEEE, Kurukshetra, India, 1– 5,.

48. Prett DM, Gillette RD (1980) Optimization and constrained multivariable control of a catalytic cracking unit. *Jt Autom Control Conf* 17:73–78,
49. Primbs JA, Nevistic V, Doyle JC (1999) Nonlinear optimal control: a control lyapunov function and receding horizon perspective. *Asian Journal of Control* 1(1):14–24,
50. Mayne D, Rawlings J (2001) Correction to "constrained model predictive control: stability and optimality". *Automatica* 37(3):483,
51. Mayne DQ (2014) Model predictive control: Recent developments and future promise. *Automatica* 50(12):2967–2986,
52. Mayne DQ, Rawlings JB, Rao CV, Scokaert P (2000) Constrained model predictive control: Stability and optimality. *Automatica* 36(6):789–814,
53. McKinnon CD, Schoellig AP (2019) Learn fast, forget slow: Safe predictive learning control for systems with unknown and changing dynamics performing repetitive tasks. *IEEE Robotics and Automation Letters* 4(2):2180–2187,
54. Schmitt L, Keller M, Albin T, Abel D (2020) Real-time nonlinear model predictive control for the energy management of hybrid electric vehicles in a hierarchical framework. *2020 Am Control Conf (ACC), Denver, CO, USA*, 1961–1967,
55. Schubert P, Stemmler S, Abel D (2019) Towards predictive anti-sway control of hanging loads: model-based controller design for a knuckle boom crane. *In: 2019 18th European Control Conference (ECC), IEEE, Naples, Italy,* 2276–2282,
56. Schwenzer M (2021) Closing the loop of model predictive force control in milling with ensemble Kalman filtering. *PhD thesis RWTH Aachen University. Aachen, Germany* 112.
57. Schwenzer M, Adams O, Klocke F, Stemmler S, Abel D (2017) Model-based predictive force control in milling: determination of reference trajectory. *Prod Eng.* 11(2):107–115,

58. Serale G, Fiorentini M, Capozzoli A, Bernardini D, Bemporad A (2018) Model predictive control (MPC) for enhancing building and HVAC system energy efficiency: Problem Formulation, Applications and Opportunities. *Energies* 11(3):631,
59. . Shaltout ML, Alhneaish MM, Metwalli SM (2020) An Economic Model Predictive Control Approach for Wind Power Smoothing and Tower Load Mitigation. *Journal of Dynamic Systems, Measurement, and Control* 142(6):061005,
60. Shekhar RC, Manzie C (2015) Optimal move blocking strategies for model predictive control. *Automatica* 61:27–34,
61. Shen C, Shi Y, Buckham B (2018) Trajectory tracking control of an autonomous underwater vehicle using Lyapunov-based model predictive control. *IEEE Transactions on Industrial Electronics* 65(7):5796–5805,
62. . Wu Z, Rincon D, Christofides PD (2020) Process structure-based recurrent neural network modelling for model predictive control of nonlinear processes. *Journal of Process Control*, 89:74–84,
63. Xie S, Hu X, Xin Z, Brighton J (2019) Pontryagin's Minimum Principle based model predictive control of energy management for a plug-in hybrid electric bus. *Applied Energy* 236:893– 905,
64. Yin X, Jindal A, Sekar V, Sinopoli B (2015) A control-theoretic approach for dynamic adaptive video streaming over http. *In: Proc. 2015 ACM Conf. Special Interest Group on Data Com. - SIGCOMM '15, ACM Press, London, United Kingdom*, 325–338,
65. Yin X, Wang X, Liu X, Chi R, Lin M, Wang Y (2018) An iterative learning model predictive control strategy for evaporator. *In: 2018 37th Chinese Control Conference (CCC), IEEE, Wuhan,* 3652–3656,

66. Yoon S, Jeon H, Kum D (2019) Predictive cruise control using radial basis function network-based vehicle motion prediction and chance constrained model predictive control. *IEEE Transactions on Intelligent Transportation Systems,* 20(10):3832–3843,

67. Yu N, Salakij S, Chavez R, Paolucci S, Sen M, Antsaklis P (2017) Model-based predictive control for building energy management: Part II – experimental validations. *Energy and Buildings* 146:19– 26,

68. Zhang HT, Wu Y, He D, Zhao H (2015) Model predictive control to mitigate chatters in milling processes with input constraints. *Int J Machine Tools Manuf,* 91:54–61,

69. Zhang X, Bujarbaruah M, Borrelli F (2019) Safe and nearoptimal policy learning for model predictive control using primal-dual neural networks. *arXiv*:190608257 [cs, eess, stat] 144.

70. Zheng A, Morari M (1995) Stability of model predictive control with mixed constraints. *IEEE Trans. Autom Control,* 40(10):1818–1823,

71. Zhongjun X, Mengxiao W (2009) Time-delay process Multivariable model predictive function control for basis weight & moisture content control system. *In: 2009 Chinese Control and Decision Conference, IEEE, Guilin, China,* 4089–4093,

72. Zinober A, Owens DH (2003) Nonlinear and adaptive control: *NCN4 2001. Lect. Notes Control Inform. Sci., Springer Berlin Heidelberg.*

73. Zou C, Hu X, Wei Z, Wik T, Egardt B (2018) Electrochemical estimation and control for lithium-ion battery health-aware fast charging. *IEEE Trans. Ind Electron,* 65(8):6635–6645,

74. . Zou S, Wang Z, Hu S, Wang W, Cao Y (2020) Control of weld penetration depth using relative fluctuation coefficient as feedback. *J Intell Manuf,* 31 :1203–1213,

75. Waldrop MM (2016) The chips are down for Moore's law. Nature 530(7589):144–147.

76. Qin S, Badgwell TA (2003) A survey of industrial model predictive control technology. *Control Eng. Pract*, 11(7):733–764,

77. Wu Z, Rincon D, Christofides PD (2020) Process structure-based recurrent neural network modelling for model predictive control of nonlinear processes. *Journal of Process Control,* 89:74–84.

78. Uys, P. E., Els, P. S., Thoresson, M., (2007), Suspension settings for optimal ride comfort of off-road vehicles travelling on roads with different roughness and speeds, *Journal of Terramechanics*, 44(2), 163–175.

79. Els P.S, Uys P.E, Snyman J.A, Thoresson M.J. (2006). Gradient-based approximation methods applied to the optimal design of vehicle suspension systems using computational models with severe inherent noise. *Mathematical and Computer Modelling*, 43(7-8), 787–801.

80. Elbeheiry, E.M, Karnoop, D.C (1996). Optimal control of random vibration with constrained suspension deflection. *Journal of Sound and Vibration*, 189(5), 547-64.

81. Mastinu, G., Gobbi, M. (2001). Analytical description and optimization of the dynamic behaviour of passively suspended road vehicles. *Journal of sound and vibration*, 245(3), 457-48.

82. Lozia, Z. (1991). Analysis of vehicle behaviour during lane change maneuver on an uneven road surface. *Vehicle system dynamics*, 20(sup-1), 417-431.

83. Marzaband, J., Goodarz, A., Zohoor, H., Hojjat, Y. (2004). Stochastic optimal preview control of a vehicle suspension. *Journal of Sound and vibration*, 275(3-5), 973-990.

84. Tamboli, J.A, Joshi, S.G. (1999). Optimum design of a passive suspension system of a vehicle subjected to actual random road excitations. *Journal of sound and vibration*, 219(2), 193-205.

85. Kargarnovin, M.H., Younesian, D., Thompson, D., Jones, C., (2005), Ride comfort of high-speed trains travelling over railway bridges. *Vehicle System Dynamics*, 43(3), 173-197.

86. Kong, Y. S., Omar, M. Z., Chua, L. B., Abdullah, S., (2014). Ride quality assessment of bus suspension system through modal frequency response approach. *Advance Mechanical Engineering*, 269721, 17.

87. Ke, C., Jie, G., (2010), Simulation of vehicle ride comfort based on VPG. *Proc. - 3rd Int. Conf. Intell. Networks Intell. Syst.* ICINIS 2010, 323–326.

88. Yang, Y.B., Lin, C.L., Yau, J.D., Chang, D.W., (2004). Mechanism of resonance and cancellation for train-induces vibrations on bridges with elastic bearings. *Journal of Sound vibration,* 269(1-2), 345-360.

89. Lin, Y., Xin, L., Yang, C., Zou, Z. (2001). Study on dynamic response of train excited by the irregularity of track on the high speed railway bridge. *Journal of vibration and shock*, 3, 47–49.

90. Nisihiyam Lewis, C. H., Griffin M. J. (1996). The transmission of vibration to the occupants of a car seat with a suspended back-rest. *Journal of Automobile Engineering*, 210(3), 199-207.

91. Kargornovin et al Lozia, Z. (1991). Analysis of vehicle behaviour during lane change manoeuvre on an uneven road surface. *Vehicle system dynamics*, 20(sup-1), 417-431.

92. Ataei, M., Asadi, E., Goodarzi, A., Khajepour, A., Khamesee, M. B. (2017). Multi-objective optimization of a hybrid electromagnetic suspension system for ride comfort, road holding and regenerated power. *Journal of Vibration and Control*, 23(5), 782–793.

93. Mohajer, N., Abdi, H., Nelson, K., Nahavandi, S. (2017). On the simulation-based objective estimation of road vehicle ride comfort. *Mechatronic (ICM) International conference, IEEE,* 978-1-5090-4538-9/17, 159-165.

94. Boileau, P.É., Wu, X., Rakheja, S. (1998). Definition of a range of idealized values to characterize seated body biodynamic response under vertical vibration. *Journal of Sound and Vibration,* 215(4), 841-862.

95. Agostinacchio, M., Ciampa D., Olita, S. (2014). The vibrations induced by surface irregularities in road pavements – a Matlab® approach. *European Transport Research Review,* 6(3), 267–275.

96. Goncalves, F. D., (2001). Dynamic Analysis of Semi-Active Control Techniques for Vehicles Application, *M. S. Thesis, Dept. of Mechanical Engineering, Virginia Polytechnic Institute and State University, Virginia*.

97. Bemporad, A., & Morari, M. (1999). Control of systems integrating logic, dynamics, and constraints. *Automatica*, 35(3), 407–427.

98. Nguyen, M. Q., Canale, M., Sename, O., & Dugard, L. (2016). A Model Predictive Control approach for semi-active suspension control problem of a full car. *2016 IEEE 55th Conference on Decision and Control (CDC)*, 721–726.

99. Yakub, Fitri & Mori, Yasuchika. (2015). Heavy Vehicle Stability and Rollover Prevention via Switching Model Predictive Control. *International journal of innovative computing, information & control*: IJICIC. 11. 1751-1764.

100. D.Q. Mayne, S. Rakovic´, R. Findeisen, and F. Allgo¨wer,"Robust out-put feedback model predictive control of constrained linear systems," *Automatica*, vol. 42, no. 7, pp. 1217–1222, 2006.

101. Fei, Ding & Han, Xu & Zhang, Nong & Luo, Zhen. (2014). Characteristic analysis of pitch-resistant hydraulically interconnected suspensions for two-axle vehicles. *Journal of Vibration and Control*. 21. 10.1177/1077546314520829.

102. Múčka, Peter. (2018). Simulated Road Profiles According to ISO 8608 in Vibration Analysis. *Journal of Testing and Evaluation.* 46. 20160265. 10.1520/JTE20160265.

103. Jeong-Hoon Kim, Chong-Won Lee, Semi-active damping control of suspension systems for specified operational response mode, *Journal of Sound and Vibration*, Volume 260, Issue 2, 2003, Pages 307-328,

104. Gupta, Ashish & Vikas, Rastogi & Bhardwaj, Nilanjan & Upadhya, Shreyansh. (2018). Development of Hybrid Control Algorithm for Improvement of performance of Semi-Active Suspension System. *World Journal of Modelling and Simulation*. 15. 53-63.